INVESTIGATING DNA DAMAGE AND OXIDATIVE STRESS IN URTICANT PHOSGENE OXIME-INDUCED SKIN TOXICITY IN MICE

By

Omid Madadgar

A THESIS

Submitted to
Michigan State University
in partial fulfillment of the requirements
for the degree of

Microbiology and Molecular Genetics-Master of Science

2023

ABSTRACT

Phosgene Oxime (dichloroform oxime; CX), an urticant categorized as a vesicating agent, is a potential chemical threat agent. Exposure causes rapid and painful dermal injury and systemic effects leading to prompt incapacitation and death; however, its mechanism of action is unknown and effective therapies have not been identified. Since exposure to mustard vesicants has been shown to cause oxidative stress, DNA damage, and apoptotic cell death, we studied these toxic effects from CX skin exposure in mice. We exposed the dorsal skin of male C57BL/6 mice to vapor generated from 10 µl of liquid CX or 0.5 or 1.0 min using two 12 mm caps at MRIGlobal, MO. Results showed that CX skin exposure caused increased expression of DNA damage markers, phosphorylated H2A.X (Ser139) and p53 (Ser15), within 2h of exposure. Terminal deoxynucleotidyl transferase biotin-dUTP nick end labeling showed an increase in epidermal cell death within 2h of CX exposure and increased cleaved caspase 3 and cleaved Poly (ADP-ribose) polymerase 1, suggesting apoptotic cell death and rapid skin toxicity. Further investigation showed increase in oxidative DNA damage (8-oxo-2-deoxyguanosine), protein oxidation (carbonylation), and lipid peroxidation (4-Hydroxynonenal) in the skin of CX-exposed mice. In summary, this comprehensive study reports novel outcomes indicating that CX-induced apoptotic cell death could involve oxidative stress and programmed signaling leading to DNA damage. Oxidative damage and related signaling pathways could significantly contribute to CX-induced skin toxicity either directly and/or via inflammatory response and mast cell activation (reported in our recent studies), which is being further analyzed in our ongoing studies.

Dedicated to my wife, Zohreh, and my daughter, Rasta.

ACKNOWLEDGMENTS

I would like to thank my advisor Dr. Tewari-Singh for her support and guidance throughout this project. Her support was always encouraging and helped me learn experimental design and methods used in the field of toxicology. Also, I would like to thank the faculty and staff of both the Microbiology and Molecular Genetics and Pharmacology and Toxicology departments for their help and guidance. I am also grateful to my committee members for their time and efforts. I learned so much in our meetings and discussions. I would also like to thank everyone in my lab, including the lab manager; Steve Lundbeck, the undergraduate students, and the Ph.D. students; Ebenezar Okoyeocha and Andrew Roney, and the postdoctoral fellows; Satyendra Singh and Dinesh Goswami, for all their help and support. I also thank my family for their help and sacrifice. In the end, I would like to thank the National Institutes of Health for the funding support towards this project and the mice for their sacrifice in this research.

TABLE OF CONTENTS

LIST OF ABBREVIATIONS	vi
CHAPTER 1: LITERATURE OVERVIEW	1
1.1 History and classification of chemical warfare agents	
1.2 Pathways relevant to the mechanism of action of vesicating agents	
CHAPTER 2: INVESTIGATING DNA DAMAGE AND OXIDATIVE S	STRESS IN
URTICANT PHOSGENE OXIME-INDUCED SKIN TOXICITY IN MICE	13
2.1 Materials and Methods	
2.2 Results.	20
CHAPTER 3: DISCUSSION	30
3.1 Discussion	30
3.2 Future directions	35
BIBLIOGRAPHY	40
APPENDIX A: IMMUNOBLOT IMAGES	45
APPENDIX B: ANALYSIS OF IMMUNOBLOTTING	48

LIST OF ABBREVIATIONS

4HNE 4-Hydroxynonenal

8-OHdG 8-hydroxy-2-deoxyguanosine

Apaf1 Apoptosis activating factor 1

AIF Apoptosis-inducing factor

ATM Ataxia Telangiectasia Mutated

ATR ATM- and Rad3-related

BAK BCL-2-antagonist/killer

BAX BCL2-Associated X Protein

BH3 Bcl-2 Homology 3

CEES Chloroethyl ethyl sulfide

Chk1, Chk2 Checkpoint kinase 1, 2

COX2 Cyclooxygenase 2

DNPH 2,4-dinitrophenylhydrazine

DNA-PKs DNA-dependent protein kinase

DSB Double strand break

FADD Fas-associated death domain

LSD Lysergic acid diethylamide

LEW Lewisite

MDM2 Mouse double minute 2 homologs

MPO Myeloperoxidase

MRIGlobal Midwest Research Institute Global

NAC N-acetylcysteine

NADP Nicotinamide Adenine Dinucleotide Phosphate

NM Nitrogen mustard

NSAID Nonsteroidal Anti-Inflammatory Drugs

PARP Poly (ADP-ribose) polymerase 1

PAO Phenylarsine oxide

Ptch1+/- Heterozygote in Ptch tumor suppressor gene

PUMA p53 upregulated modulator of apoptosis

ROS Reactive Oxygen Species

SM Sulfur mustard

SSB Single strand break

TNFR Tumor necrosis factor receptor

TUNEL Terminal deoxynucleotidyl transferase biotin-dUTP nick end labeling

CHAPTER 1: LITERATURE OVERVIEW

1.1 History and classification of chemical warfare agents

Among the weapons of mass destruction, chemical weapons (CW) are among the most lethal weapons created by mankind and are designed to incapacitate, kill, or cause long-term detrimental injuries to the exposed population. CW are extremely toxic chemicals that can be used in military conflicts in the forms of liquid, gas, aerosol, and/or powder [1] as Chemical warfare agents (CWA). They have been utilized widely in warfare due to their inexpensive cost of manufacture, ease of synthesis, and catastrophic multi-organ toxic effects [2-4] Although the use of CWA has a long history, their use for deliberate destruction effectively began during World War I (WWI) when chlorine was used by the German army against Allied forces at Ypres [1]. Subsequently, the Allies (France, Great Britain, United States, and Russia) reacted by using chemicals for military purposes. During the 4 years of WWI (1914-18), about 1.3 million people were affected and more than 100,000 died by CW on both sides of the conflict [5]. Millions of innocent civilians were killed by the Nazis with Zyklon B gas (hydrogen cyanide gas) during World War II [1]. The only major use [1] of CW since WWI occurred during the Iran-Iraq War in the 1980s. The largest single CW attack, killing around 5,000 people, was an Iraqi nerve agent attack on the Kurdish civilian population of Halabja [1]. This attack illustrates one of the unique characteristics of CW agents that allows them to be considered weapons of mass destruction. Despite the convention on the prohibition of chemical weapons and their destruction, which was signed in 1993, a total of about 71,000 tons of chemical weapons have been declared and stockpiled in the countries like Russia, United States, Albania, India, Iraq, South Korea, Libya, and, recently, Syria [6]. Recently, the Syrian government used sarin gas on the Ghouta area of Damascus, killing more than 1,400 Syrians, many of whom were children [7].

CWA with their highly toxic properties, inexpensive nature, ease of production, and potentially inconspicuous delivery methods, are also interesting weapons for terrorist groups [1]. CWA can be dispersed as either liquids, gases, or aerosols, or absorbed into particles such as powders causing devastating long-term or lethal effects. Continued technological advancements, in the context of the current geopolitical climate, could result in chemical terrorism becoming a serious threat that could easily eclipse that of firearms[1].

CWA are classified according to their mechanism of toxicity in humans into 1) vesicant/blister agents that cause severe blistering when they come into contact with the skin, like sulfur mustard, nitrogen mustard, lewisite, and phosgene oxime; 2) nerve agents such as organophosphorus compounds which inhibit the enzyme acetylcholinesterase, like the G series (e.g., tabun, sarin) or V series (e.g., VE, VX); 3) blood agents that cause tissue hypoxia physically, like nitrogen gas or chemically, like cyanogen chloride and arsine by interfering with oxygen transport; 4) choking agents or pulmonary damaging agents which are toxic to the human lung when inhaled, like phosgene chloropicrin; 5) riot control agents, such tear gases, chlorobenzylidenemalononitrile, and diphenylaminoarsine; and 6) incapacitating/behavioraltering agents or psychomimetic agents such as carfentanil and lysergic acid diethylamide (LSD-25) [1, 8]. The vesicant phosgene oxime is the focus of this study.

Vesicants and Phosgene Oxime

Vesicants are chemicals with the ability to cause dermal vesicles/blisters and lead to acute and debilitating injuries to the mucus membranes and internal organs (4). These include 1) mustard vesicating agents such as sulfur mustard [SM; bis(2-chloroethyl) sulfide, HD] and nitrogen mustard [HN1 (bis (2 chloroethyl) ethylamine)]; 2) arsenical vesicants such as lewisite (L; LEW; dichloro (2 chlorovinyl)); and 3) nettle agent phosgene oxime (dichloroformoxime; Cl2CNOH).

Among these, SM has been the most extensively used in different conflicts for over 100 years, which has earned it the nickname of the "King of The Battle Gases" [4]. Figure 1 compares the chemical structure of these three vesicant warfare agents and table 1 compares some of their important characteristics.

Figure 1: Chemical structures of vesicants. (A) mustard vesicant SM, (B) arsenical vesicant LEW, and (C) Nettle vesicant CX.

Chemical agent		Pain	Tissue dam	age	Blister
Mustard: Sulfur Mustard (SM), Nitrogen Mustard (NM). (HN- 1,2 and 3) Lewisite (L): Arsenicals			Onset of clinical effects is hours (24h) Seconds to minutes		Fluid filled Fluid filled
· Mustaru gas.	❖ Lewisi			* Phosgene Oxime:	
 Most commonly used. First reported use in 1917. King of the battle gasses. 	❖ D❖ N	 ★ First synthesized in 1929. ★ Although stockpiled during World II, there are no records of its use in battlefield. ★ Recently found CX in Oklahoma, ★ No surrogate for research. ★ Mechanism is unknown. 			uring World War of its use in Oklahoma, 2019 rch.

Table 1: Vesicant chemical warfare agents and the history of their synthesis and usage in the battlefield [4].

Phosgene Oxime (CX) is a halogenated oxime and nettle agent that causes urticaria (despite its classification as a vesicant it does not cause blisters/vesicles). CX is colorless in its solid form, but its color in impure samples often changes to yellowish-brown in its liquid form with a melting

point of 39- 40°C and a boiling point of 128°C at 76 mm of Hg. It has a strong, unpleasant, disagreeable odor and is a violently irritating vapor. CX is also very unstable, reactive (soluble in water and organic solvents and hydrolyzes very quickly), and volatile (1800 mg/m3 at 20°C). It is heavier than air but does not persist in the environment for a long time and its half-life is 83 days at unspecified pH and temperature. CX can be synthesized by the reduction of chloropicrin with tin in the presence of hydrochloric acid [9-11].

$$C13CNO2 + 2 Sn + 5 HC1 + H2O \rightarrow C12C=N-OH + 2 H3O[SnC13]$$

Although the use of CX in warfare has not been reported, it was first produced in Germany in 1929 and is reported to have been developed by both Germany and Russia and stockpiled during World War II as a potent chemical weapon [11]. Recently an FBI investigation has found CX inside a Lawton home in Oklahoma (March 20th 2019, https://www.news9.com/story/40170458/fbi-investigationfinds-chemical-warfare-agent-inside-lawton-home).

Due to its easy synthesis, storage, and chemical properties, CX is considered as a potential emerging chemical threat. When exposed, CX produces acute pain, excruciating itching, and a rash resembling hives. These symptoms culminate in violent reactions and serious tissue damage [11]. CX penetrates cloth and rubber more quickly than other chemical agents while also having the ability to be mixed with other chemical agents, increasing their penetration, and causing the quick onset of severe and prolonged effects [11, 12]. Exposure to CX, more so than the other vesicant agents due to its fast penetration, results in instant pain and tissue destruction, leading to dermal, ocular, and pulmonary damage even at low doses, while high doses have multiorgan toxic effects with mortality [12]. It is suggested that CX is rapidly absorbed through the skin, leading to immediate skin irritation, itching, pain, skin blanching (whitening), erythema, edema, and hives formation, which has been shown for the first time, in our reported studies [10]. After minutes to

an hour, the exposed area is edematous, which resolves within a day with dark pigmentation and severe necrosis. Healing takes weeks to months and severe systemic toxicity may also occur. CX is the most potent and dangerous chemical threat agent among vesicants; however, information on its dermal absorption and effects on human skin tissue, injury, and mechanism of action is lacking and treatments have not been identified [10-12].

The dermal urticaria from CX is similar to allergic and non-allergic reactions to certain environmental substances and contact dermatitis, which is believed to be mainly caused by mast cell activation and subsequent release of inflammatory mediators [10]. It is possible that CX has alkylating and nucleophilic properties, and its toxic effects are caused by its breakdown products. It is also suggested that CX involves a direct effect involving corrosive injury, cell death, and tissue destruction and an indirect effect due to inflammation and recruitment of neutrophils and macrophages, and oxidative stress, which could lead to delayed tissue injury [10, 12].

1.2 Pathways relevant to the mechanism of action of vesicating agents

DNA damage and Apoptosis

DNA damage has been shown as one of the prompt and key toxic effects of mustard vesicating CWA and they have been shown to cause an increase in the phosphorylation of DNA damage markers H2A.X and p53 as well as p53 accumulation upon cutaneous exposure [13-15]. Pilot studies on dermal CX exposure in hairless mice showed apoptotic cell death in the basal epidermal keratinocytes at 8 h post-exposure that could be mediated by the DNA-damaging effect of CX as shown by increased p53 phosphorylation (Ser15) and its accumulation [10]. p53 phosphorylation and its accumulation can affect cell cycle progression, inducing transcription of cyclin-dependent kinase inhibitor p21 [16, 17]. Phosphorylation of p53 at ser15 by the ataxia telangiectasia mutated (ATM) protein kinase, regulates cell cycle checkpoint and is phosphorylated by double-strand

breaks in DNA and is an important marker for DNA damage. P53 phosphorylation stabilizes and inhibits mouse double minute 2 homolog (MDM2) thereby preventing its degradation via ubiquitination. The p53-MDM2 loop modulates the DNA damage response, and P53 phosphorylation and accumulation indicate DNA damage (Fig. 2) [18] (Fig. 2: modified from reference 42).

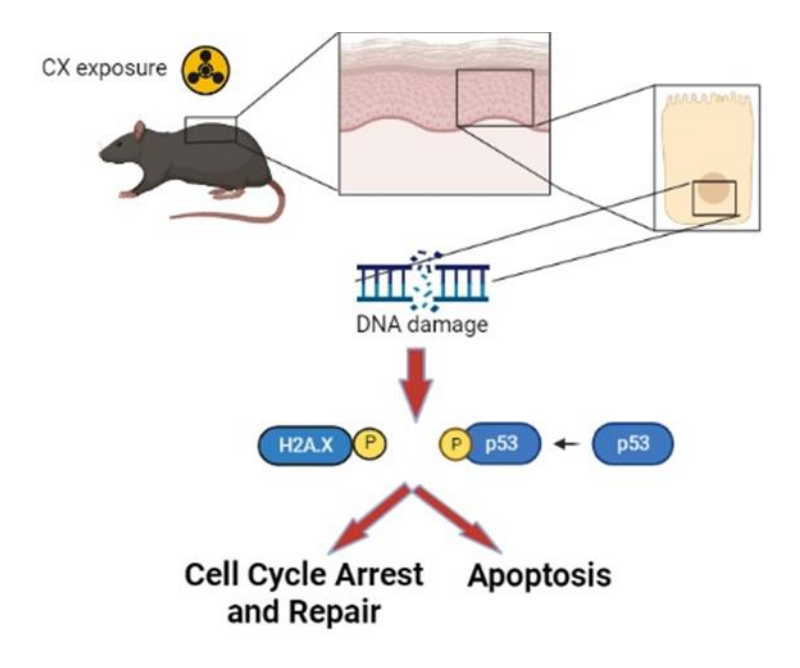


Figure 2: Schematic representation of the possible DNA damage effects after CX exposure. DNA damage due to CX exposure can phosphorylate p53 (Ser 15) and H2A.X (Ser 139), which ultimately induces cell cycle arrest and DNA repair or, on the other hand, causes cell death.

One of the other important proteins in the DNA damage response (DDR) pathway and the detection of DNA damage is histone H2A.X [19]. In response to DNA double-strand breaks, ATM and/or DNA-dependent protein kinase (DNA-PK) phosphorylate histone H2A.X at Ser139 to form γH2A.X. The formation of γH2A.X foci on DSB sites is the earliest and the critical event indicating DNA damage, which is observed in studies with mustard vesicating agents and CX dermal exposure [10, 19, 20]. The cytotoxicity of mustard vesicating agents is also attributed to

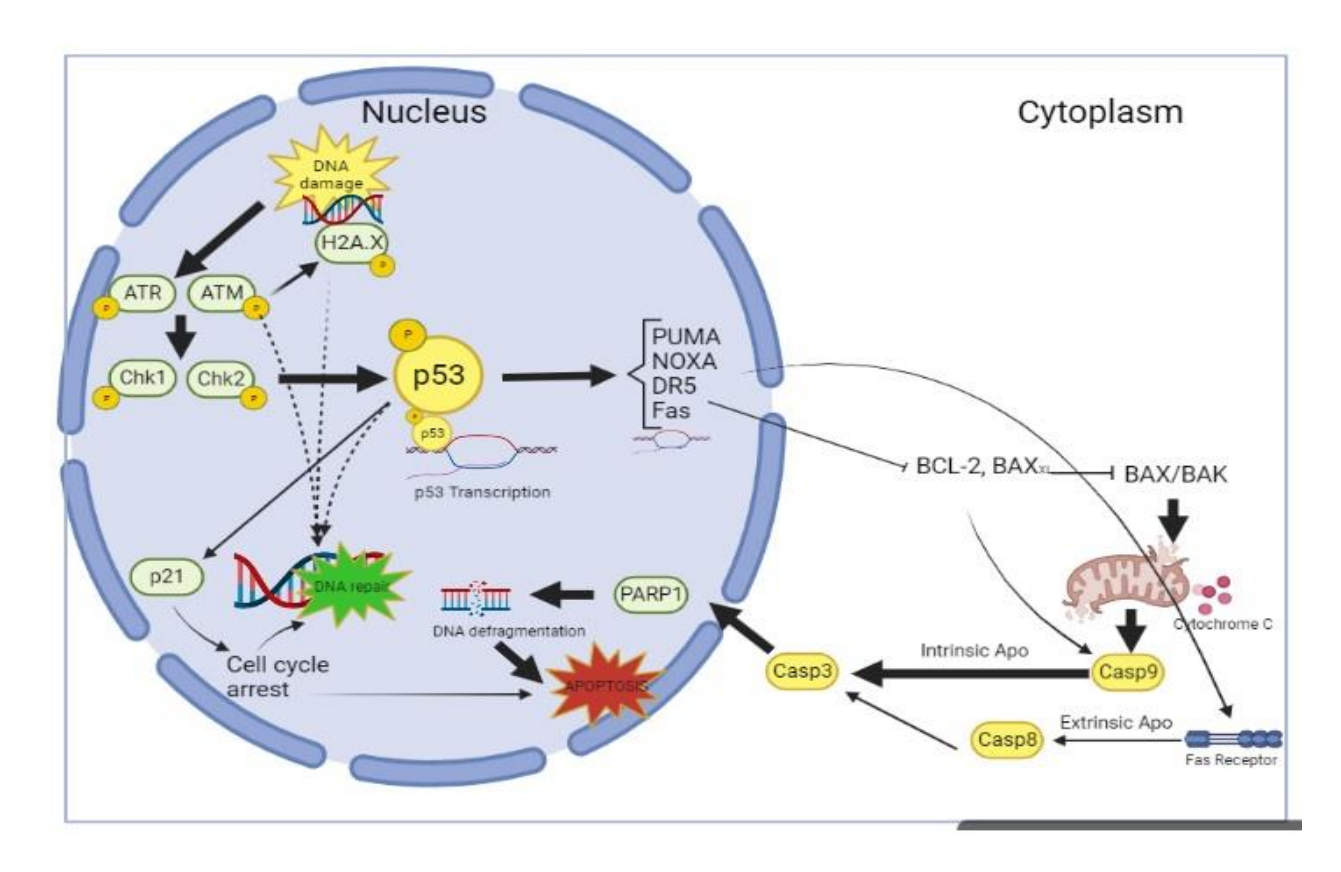


Figure 3: DNA damage induces p53 phosphorylation and its activation, leading the cell to either DNA repair and cell survival or apoptosis. ATM and ATR and then Chk1 and Chk2 are phosphorylated which further phosphorylates p53. Phosphorylated p53 (Ser 15) can lead the cells either to DNA repair or increase transcription of total p53. ATM also phosphorylates H2A.X which contributes later to DNA repair. On the other hand, p53 activation leads to the induction of BH3 only proteins (PUMA, NOXA etc) and unleashes pro-survival BCL2 family members (BAX, BAK), increasing apoptosis via intrinsic pathway, or activates extrinsic apoptosis via increasing FAS and DR5 ligands. The outcome of DNA damage would be DNA repair or apoptosis. Cleaved caspase 3 and PARP1 have a central role and are common molecular markers of intrinsic and extrinsic apoptosis [modified from 23, 24, 25].

their alkylating properties resulting in the formation of DNA adducts and crosslinks that can also cause cell cycle arrest and inhibition of DNA synthesis [46]

When lesions are unrepaired or the DNA repair system does not work properly, DNA damage often leads to apoptosis [21]. Phosphorylated p53 migrates to the nucleus and increases direct transcriptional activation of the pro-apoptotic bcl-2 Homology 3 (BH3) only proteins, p53 upregulated modulator of apoptosis (PUMA) and, to a lesser extent, Phorbol-12-myristate-13-

acetate-induced protein 1 (NOXA). This activation unleashes the cell death effectors BCL2-Associated X Protein (BAX) and BCL-2-antagonist/killer (BAK), which each can trigger intrinsic apoptosis by stimulating mitochondria to release cytochrome C and then cleaved caspase 9, which ultimately leads to apoptosis (Fig. 3). Apoptosis is the programmed cell death mechanism to ensure cell integrity and homeostasis [22]. Although a large necrotic area is observed in clinical and histopathological evaluations, apoptosis as a reversible mechanism has additional importance regarding treatment measures and strategies [10]. Figure 3 shows DNA damage response through p53 transcription and phosphorylation leads the cell to DNA repair or apoptosis (Fig. 3 modified from reference [23-25])

Apoptosis occurs via extrinsic and intrinsic pathways. The extrinsic pathway is mediated by death receptors within the TNFR (tumor necrosis factor receptor) superfamily by activation of one of the death receptors followed by FADD (Fas-associated death domain) as well as activation of additional adaptor proteins, then caspase 8 cleavage, and, finally, proteolytic cleavage and activation of the effector caspases, caspases-3, -6 and -7 [26]. On the other hand, the intrinsic pathway, mediated by the release of apoptogenic factors of AIF (apoptosis-inducing factor) or cytochrome C from the mitochondria, depends on the apoptotic stimulus as well as on the balance of members of the Bcl-2 family of proteins [26]. Cytochrome C and ATP/dATP bind Apaf1 (apoptosis activating factor 1) in the cytosol to form the heptameric apoptosome, which activates the initiator procaspase-9. Procaspase-9 activates the executioner caspases, 3, 6, and 7. Caspases 3 and 7 also cleave Poly (ADP-ribose) polymerase (PARP1), generating 89-kDa and 24-kDa PARP1 fragments. The 89-kDa PARP1 fragments, which are covalently attached PAR polymers, are translocated to the cytoplasm and AIF binding to PAR attached to the 89-kDa PARP1 fragment facilitates its translocation to the nucleus and associates with DNase, resulting in large-scale DNA

fragmentation. Thus, the 89-kDa PARP1 fragment is a PAR carrier to the cytoplasm, inducing AIF release from mitochondria, which triggers apoptosis [26, 27]. Cleaved caspase 3 (the central executioner caspase) and cleaved PARP1 are considered useful markers to study apoptosis in many studies including vesicant-induced skin cell toxicity [28, 29] (Fig. 3).

Inflammation and oxidative stress

Exposure to vesicants is associated with inflammation, which plays an important role in their toxicity [4, 30]. Also, the toxicity response and skin urticaria from CX resembles anaphylactic reaction and urticaria from allergic reactions, which involve an inflammatory response mainly due to mast cell activation [10]. It is known that mast cells not only release proinflammatory mediators and cytokines but also produce intracellular reactive oxygen species (ROS), which altogether can stimulate the production of proinflammatory cytokines, participate in the regulation of innate immunity, and lead to DNA damage. Mast cells recruit immune cells like neutrophils and macrophages to the exposure site, which could also increase ROS, by releasing NADPH oxidase and other enzymes [10, 30-34]. Cyclooxygenase-2 (COX2) is an enzyme involved in the conversion of arachidonic acid to prostaglandin H2, an important precursor of prostacyclin, which is expressed in inflammation. COX2 is not expressed under normal conditions in most cells, but elevated levels are found during inflammation, and is the target of NSAIDs (Nonsteroidal antiinflammatory drugs) to decrease inflammation [35]. Apart from inflammation, production of ROS could result from electrophilic or oxidative stress with depletion of cellular detoxifying thiol levels including glutathione. Hence, therapies that can target oxidative stress pathways may represent important candidates for reducing vesicant-induced tissue injury [36].

The mode of DNA and other biomolecular damage is not completely understood in CX toxicity. Since other vesicants trigger several molecular and cellular pathways to cause oxidative stress resulting in DNA damage, oxidative damage could be one of the possible mechanisms for CX-induced DNA damage [4, 22, 37]. ROS-induced damage to macro-molecules includes DNA oxidation, which can inhibit replication and repair processes, lipid peroxidation, which can yield reactive electrophilic lipid peroxidation end products, and protein oxidation, which can alter the functional activity of enzymes and structural proteins [36]. ROS react with the nucleotides in DNA and make single- and double-strand breaks (SSBs, DSBs) by increasing DNA oxidation and producing DNA adducts like 8-oxo-dGs (8-OHdG). These SSBs and DSBs are sensed by ATM and ataxia telangiectasia and Rad3-related protein (ATR) and activate p53 and cause cell cycle arrest. P53 also causes apoptosis in non-transformed cells by directly activating the pro-apoptotic BH3-only proteins PUMA and NOXA through transcriptional activation [38-40] (Fig. 3).

Oxidative stress generated by exposure to toxicants like UVB radiation and vesicants, like SM and NM, oxidates not only the DNA but also other macromolecules, such as lipids and proteins [37, 41]. Numerous harmful breakdown products produced by lipid peroxidation, including malondialdehyde and 4-HNE (4-Hydroxynonenal), can bind to proteins, phospholipids, and DNA in the compartments of the cell and create covalent adducts [37, 42]. The lipid peroxides can lead to loss of membrane function, membrane fluidity, and finally membrane integrity.

Protein structure is also vulnerable to oxidative stress. Lysine, arginine, and proline undergo oxidation, which results in the creation of carbonyl derivatives that influence the biological activity of native proteins in biological systems [43]. Numerous studies have used the presence of carbonyl groups to gauge the extent of protein oxidative degradation in various in vivo settings. Oxidative stress conditions allow carbonyl groups to react with DNPH (2,4-dinitrophenylhydrazine) and form stable hydrazone derivatives which can be detected by a specific antibody [43, 44] (Fig. 4).

Skin damage including erythema, necrosis, and inflammation following cutaneous exposure to CX and mustard vesicants, e.g., SM and NM, is similar; however, CX also causes severe skin injury with immediate urticaria and blanching as well as mortality [10, 41, 45].

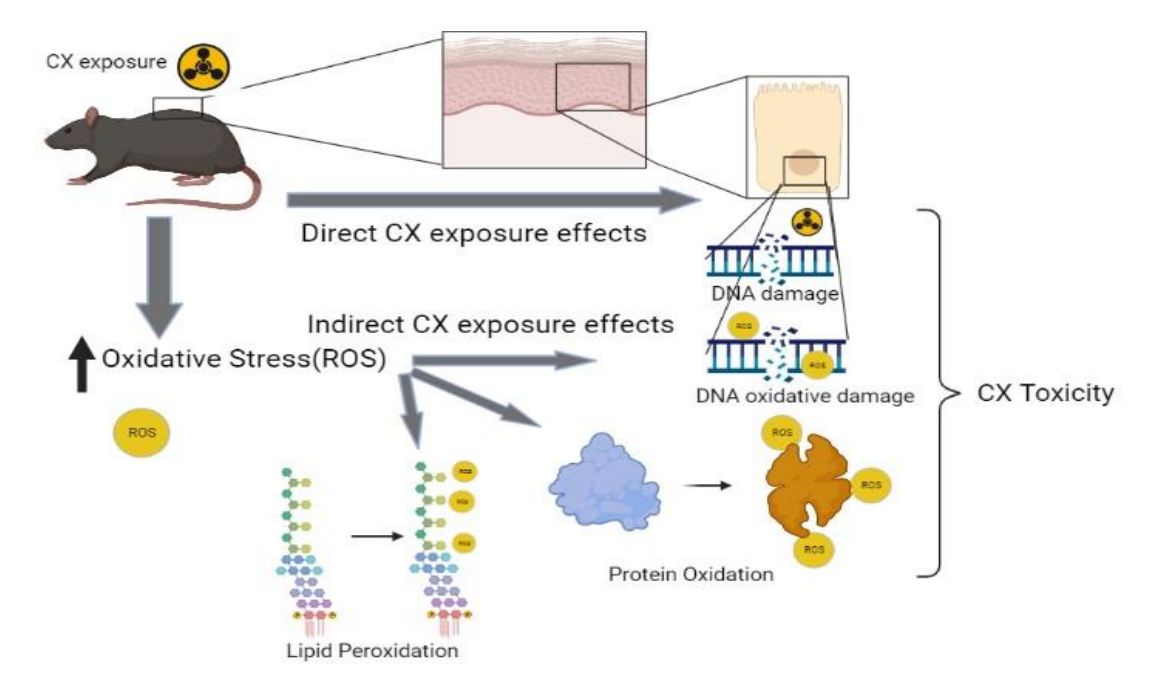


Figure 4: Schematic representation of the possible CX exposure-induced DNA damage which can be direct or via oxidative stress. Model for possible effect of CX on DNA damage. Similar to other vesicants, CX may cause direct DNA damage and/or DNA damage as well as damage to lipids and proteins via oxidative stress in the cell leading to toxicity.

DNA-damaging properties of CX could resemble mustard vesicants and its toxic effects could be via direct corrosive tissue destruction and oxidative stress due to ROS generation as well as depletion of glutathione or indirectly involve oxidative stress via an inflammatory response leading to tissue injury [12]. Earlier published pilot study from our lab suggested that CX exposure could lead to DNA damage and mast cell activation accompanied by an inflammatory response resulting in the skin toxicity [6]. However, this study was conducted only at one early time point and comprehensive studies are needed to understand the injury mechanism of the rapid onset of severe and prolonged effects of CX skin exposure to establish molecular biomarkers of skin toxicity related to DNA damage and identify therapeutic targets [10].

Based on the published mechanism of action of vesicating agents and our preliminary studies with CX, we hypothesize that CX skin exposure causes oxidative stress that could activate signaling pathways resulting in CX-induced DNA damage, apoptosis, and skin toxicity [14, 37, 41].

The objective of this study is to examine the mechanism of action and elucidate the DNA damage and oxidative stress response following CX dermal exposure in a comprehensive study in mice. The outcomes will represent the first major insight into CX-induced skin toxicity and cell death mechanisms to identify novel targets that could be explored for therapeutic intervention. We used male C57BL/6 mice as the animal model for our study since the established biomarkers here will allow us to employ mast cell knockout mice (generated in this background) to further reveal the role of mast cells in CX induced oxidative stress, DNA damage and skin toxicity. The aims of this study are to:

- 1. Examine the toxic skin effects of CX and assess the apoptotic cell death and DNA damage responses.
- 2. Investigate the oxidative stress response and related damage to biomolecules in the skin toxicity caused by CX exposure.

The outcomes from this study will identify the DNA damage and oxidative stress response that could lead to cell death and skin toxicity from CX exposure using biological and molecular markers. This study will assist in further identification of signaling pathways in CX-induced acute and prolonged skin toxicity.

CHAPTER 2: INVESTIGATING DNA DAMAGE AND OXIDATIVE STRESS IN URTICANT PHOSGENE OXIME-INDUCED SKIN TOXICITY IN MICE

2.1 Materials and Methods

Chemicals and reagents

Hematoxylin and eosin stains were obtained from Sigma–Aldrich Chemicals Co. (St. Louis, MO). The DeadEnd Colorimetric terminal deoxynucleotidyl transferase (TDT)-mediated dUTP-biotin nick end labeling (TUNEL) staining kit was obtained from Promega (Madison, WI). The detergent compatible (DC) protein assay kit was purchased from Bio-Rad Laboratories (Hercules, CA). Primary antibodies for phosphorylated p53 (Ser15); total p53, beta-actin, cleaved Caspase 3, and PARP I antibodies; horse anti-mouse IgG and anti-rabbit IgG secondary antibody labeled with horseradish peroxidase (HRP) were obtained from Cell Signaling Technology (Beverly, MA). Primary antibodies for phosphorylated H2A.X (Ser139) and 8-OHDG were purchased from Abcam Inc. (Cambridge, MA). The protein carbonylation assay kit was obtained from Abcam (Cambridge, UK) and the primary antibody for 4-HNE detection was obtained from Novus Biologicals (CO, USA). Chemiluminescence reagent ECL detection kit was purchased from Amersham Biotech, EDTA was from Thermofisher scientific (MA), Bio-Rad DC protein assay kit was obtained from Bio-Rad Laboratories (Hercules, CA), rabbit IgG antibody was from DAKO (Carpinteria, CA), CX for this study was prepared by MRIGlobal, Kansas City, MO.

Study design and dermal exposure

Male C57BL/6 mice (4-6 weeks: n=5) were obtained from Jackson Laboratories (Bar Harbor, ME), and kept under standard conditions at MRIGlobal. The animals were acclimatized for 1 week before starting exposure and were shaved using clippers 2 days before the CX exposure. The mice were anesthetized using ketamine and xylazine (IP) before exposure, and the pain was alleviated using 0.05–0.1 mg/kg subcutaneous (SC) injection of buprenorphine 30 min before CX

exposure. Then, mice were exposed to vapor (under a modified exposure system (Fig. 5)) from 10 μl neat liquid CX (95% purity) at two durations of exposure: short (0.5 min) and long (1 min) using a vapor cap (two 12 mm vapor cap exposures at each side of the dorsal skin of the mice). The calculated CX vapor dose was 2.04 mg/μl for 1 min and 1.02 mg/μl for 0.5 min skin exposure. CX preparation, exposures, and clinical assessments were conducted with standard operating procedures (SOPs) and approved Institutional Animal Care and Use Committee (IACUC) protocol as well as safety procedures at MRIGlobal. Animals were then euthanized at 24 h, 3 days, and 14 days post-exposure in the 0.5-min exposure group, and 2 h and 24 h, in the 1-min exposure group. For each time point, mice were sacrificed, and the skin was punched and harvested. Portions of each tissue were snap-frozen and other portions were fixed in 10% formalin (Fig. 6) and shipped to MSU for further analysis.

A CX exposure system was designed at MRIGlobal, Kansas City, MO to maintain temperature to obtain CX liquid test conditions. As shown in figure 5, using a heat gun and through a delivery pipe, heated air was entered at controlled rates into the box and its temperature was maintained at approximately 40°C. On either side of the dorsal midline of the back, animals were exposed to two vapor caps containing filter papers. Each filter was saturated with 10 ul of CX and animal skin exposed for either 30 seconds or 1 min. The animal was kept in the box for 2 min.

Evaluation of apoptotic cell death by TUNEL assay

Terminal deoxynucleotidyl transferase (TdT) dUTP NickEnd Labeling (TUNEL) staining was performed to detect nicks in DNA showing apoptotic cell death in the skin epithelial layer as described previously [45, 46]. Briefly, slides prepared from paraffin-embedded tissue sections were deparaffinized and rehydrated using a graded alcohol series. Following slide fixation in 4%

paraformaldehyde in PBS, sections were treated with a proteinase K solution, and labeling was carried out by including an enzyme reaction mix for terminal deoxynucleotide transferase

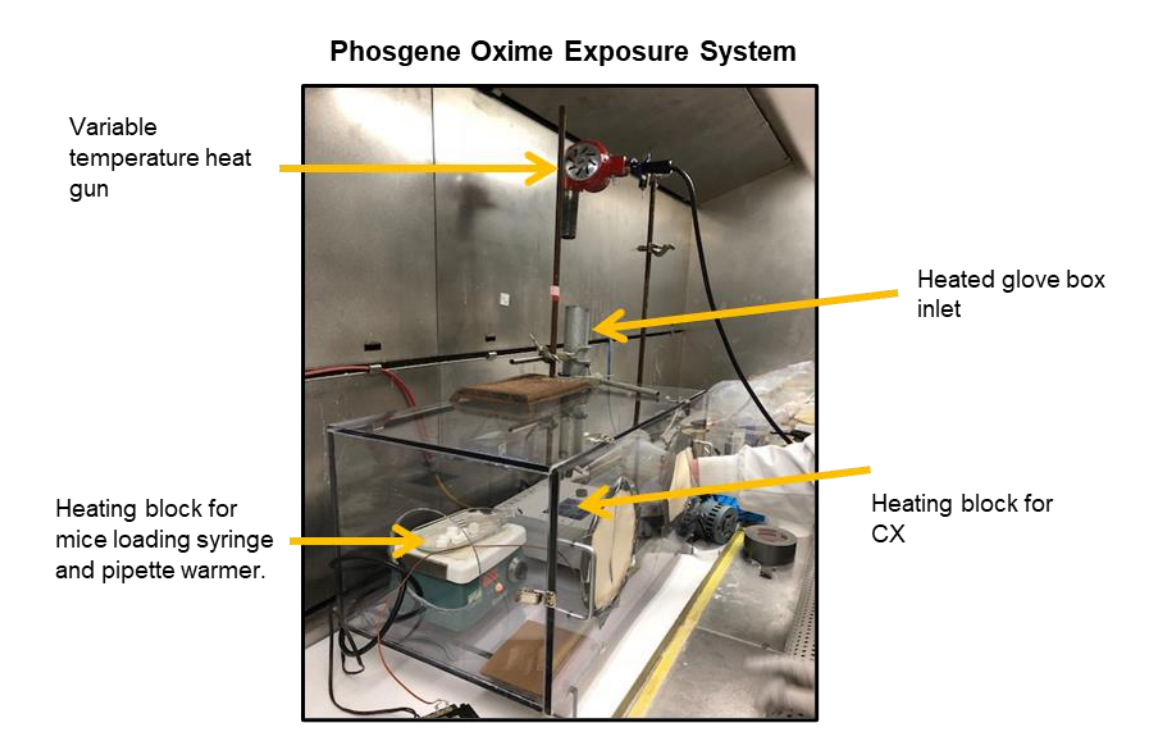


Figure 5: Phosgene oxime exposure system designed at MRIGlobal, Kansas City, MO. To maintain temperature to obtain CX liquid test conditions, the box is modified for the introduction of the heated air which is introduced into the system through a delivery pipe at controlled rates with a heat gun for temperature regulation. The glove box temperature was maintained at approximately 40°C. Once in the box, animals were exposed to two vapor caps containing filter papers on each side of the dorsal midline of the back. Each filter was saturated with 10 ul of CX with one cap placed on each side of the dorsal midline of the back, for a duration of either 30 seconds or 1 min. The animal was kept in the box for no more than 2 min but was kept under the laminar hood for at least 30 mins.

(TdT). Color development for the localization of labeled cells was performed by incubating the slides with 3,3-diaminobenzidine (DAB). Nonapoptotic cells were stained with counterstain Hematoxylin. A light microscope was used to capture images of the stained tissue. Finally, the brown colored (TUNEL positive) cells in the blue (normal cell) background were counted by a blinded investigator in 10 randomly selected fields under 400× magnification, and an apoptotic cell percentage was calculated as the ratio of apoptotic to normal cells.

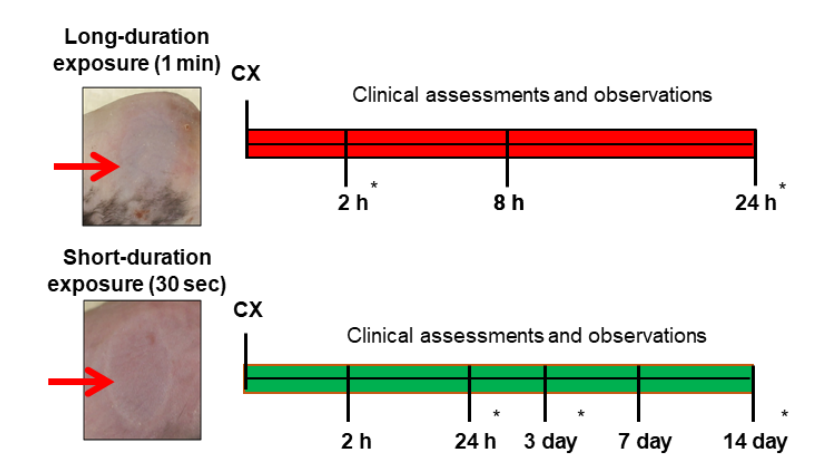


Figure 6: CX exposures and study paradigm. *, time points at which mice were euthanized and skin collected for histopathological and molecular analysis. Red arrows indicate lesions caused by exposure to CX on the skin of mice.

Immunoblotting of Apoptosis and DNA damage molecular markers

Skin tissues were lysed and whole-cell extracts were prepared using a standardized protocol in the laboratory [47]. Cell lysates were prepared in NP40 cell lysis buffer [50mM Tris-HCl (pH 7.4), 150mM NaCl, 1%NP-40, and 5mM EDTA. 25-50 mg of skin tissue was cleaned by removing subcutaneous fatty tissue on ice-cold PBS, minced, and, after adding 250-500 μl NP40 cell lysis buffer and 100X protein inhibitor cocktail (Thermo Fischer Scientific, MA, USA), left for 15 min on the ice. Then it was homogenized using a tissue homogenizer at 5000 rpm for 2-3 min and left on ice for another 15 min. Thereafter, homogenized samples were freeze-thawed twice (freeze at -80°C for 10-15 min and thaw at 37°C for 1-2 min) and finally centrifuged two times at 14000 rpm, one for 5 min and the other one, for 30 min at 4°C, with the supernatant from the second centrifugation being collected as the cell lysate. Protein concentration in the lysates was determined using a Bio-Rad DC protein assay kit. For immunoblot analyses, samples with even protein measures (40–100 μg of protein lysates per sample) were denatured in 2X or 4X SDS–PAGE sample buffer, loaded on to SDS–PAGE on 8-12% Tris–glycine gels, transferred to

nitrocellulose membranes, and then blocked for 1 h with 5% nonfat dry milk or 5% BSA. The membrane was then incubated with the appropriate concentration of primary antibodies overnight at 4°C and after washing, incubated with HRP-conjugated secondary antibodies (1/5000 for all proteins) for 2 h, and then washed again. Then, after the addition of ECL detection kit, the chemiluminescent signal was analyzed using LI-COR Odyssey FC imager. The same membrane was used to blot β-actin as the internal control to test sample homogeneity after reprobing. Western blot band density was measured using ImageJ software. After normalizing each band with their related β -actin band density, this normalized fold change was divided with the fold change of band densities of the control mice counterpart to its β -actin. Three CX exposed mouse skin samples were analyzed employing this method at each study time point and then the average and standard error of mean (SEM) of the obtained fold changes of these skin samples from each study time point compared to control were calculated (The fold change of the control samples was considered as 1 to calculate fold change of each exposed sample related to its control). Then the average and SEM at each time point compared to control (which its average was considered 1) was calculated using a one-way ANOVA statistic test to find significant differences. P<0.05 were considered statistically significant.

Oxidative DNA damage by 8-OHDG staining

Oxidative DNA damage was quantified by Immunohistochemistry (IHC) of skin sections with anti-8-OHdG using method reported earlier [48]. Mouse skin sections were blocked with 3% H_2O_2 for peroxidase activity and with 1% BSA for non-specific antigens and then were incubated with mouse monoclonal anti-8-OHdG antibody in PBS overnight at 4 °C in a humidity chamber as reported earlier. The N-Universal negative control rabbit IgG antibody was used as a negative control. Also, positive 8-OHdG slides from slides of CX exposed sample from the pilot study on

SKH-1 mice and negative control mice slides were used as biological positive and negative controls. Thereafter, following washing steps, the sections were incubated with the appropriate HRP-conjugated anti-mouse secondary antibody for 2 h, and after some washing steps, stained with DAB as the substrate for HRP. Sections were then counterstained with hematoxylin (1:10) followed by dehydration steps and mounted for microscopic observation. Positive results were defined as brown-colored DAB-positive nuclei that were counted by a blinded investigator from slides of all mice groups in 10 randomly selected fields (X400 magnification). GraphPad Prism version of 8.2.0 was used to statistically analyze the IHC data (GraphPad Software, San Diego, CA).

Lipid peroxidation by 4HNE assay

Skin tissue lysates were prepared and SDS PAGE and western blot were performed according to the protocol used for detecting other proteins, except using primary anti-4-Hydroxynonenal (4HNE) with the concentration of 1/5000 to detect 4-HNE-adducted protein modifications on protein extracts of C57BL/6 mice skin samples [37, 41]. The same membrane was used to blot β-actin as the internal control to test sample homogeneity after reprobing. The density of the bands in the entire lane of each western immunoblot of exposed skin samples was used for the calculation of fold change and comparison with its control, employing the method explained above under the in the immunoblotting method section.

Protein oxidation (Carbonylation) assay

The Protein Carbonyl Assay kit was employed for western blot analysis of oxidative modifications of protein following the manufacturer's protocol. The protein lysate (10-20 µg) was denatured by adding 12% sodium dodecyl sulfate (SDS) to a final concentration of 6% SDS. The protein samples were then derivatized with 2,4-dinitrophenylhydrazine (DNPH) solution.

Derivatization-control solution was added to the aliquot designated as the negative control instead of the DNPH solution and all were incubated for 15 min. Then the reaction was stopped by adding the neutralizing solution to both samples. The derivatized samples and the negative control were then loaded on the 12% SDS-polyacrylamide gel for electrophoresis and blotted onto a nitrocellulose membrane. The membrane was blocked like in other western blot experiments, in phosphate-buffered saline containing 0.1% Tween 20 (PBS-T) and 5% nonfat dry milk for 1 h. The membrane was then incubated with the diluted primary anti-DNP antibody (Rabbit) (1:5000) in nonfat dry milk in PBS-T overnight at 4°C, as directed by the manufacturers. Afterward, the membrane was incubated for 1 h at room temperature with HRP-conjugated secondary antibody (Goat anti-Rabbit) (1:5000) in PBS-T containing 5% nonfat dry milk. Following the manufacturer's instructions, the membrane was washed in PBS-T and treated with a chemiluminescence reagent ECL detection kit [35, 37]. The density of the bands in the entire lane of each western immunoblot of exposed skin samples was used for the calculation of fold change and comparison with its control, employing the method explained above under the in the immunoblotting method section.

Statistical Analysis

According to preliminary results from the pilot study and calculation of sample size considering $\alpha = 0.05$ (two-sided), $\beta = 0.2$, and power of the test = 80%, experiments were completed using 3 replicate samples and two technical repeats. A one-way ANOVA was used followed by a Tukey's multiple comparisons to test the significance between exposure time points and their respective controls. Statistical analysis was performed using Prism (GraphPad Software Inc., USA). p-values <0.05 were considered statistically significant.

2.2 Results

CX skin exposure increased apoptotic cell death

Based on the studies on other vesicants and our previous studies with CX [49], we examined the presence of apoptotic cells and the extent of the apoptosis in C57BL/6 mice after both short- (0.5 min) and long-duration (1 min) CX exposures in the skin epidermal cells. Pyknotic nuclei as a hallmark of apoptotic cells and brown stained apoptotic cells were observed clearly in the TUNEL-stained skin sections (Fig. 7). CX skin exposure for 1 min showed a significant increase of more than 50% apoptotic cells after 2 h of CX exposure that persisted up to 24 h post-exposure (Figs. 7A and B). CX exposure for 0.5 min resulted in around 50% and 42% apoptotic cells at 24 h and 3 days post-exposure, respectively, which was significantly higher than in control mice (Figs. 7C and D). Altogether, CX skin exposure caused a significant exposure duration-dependent increase in apoptotic cell death which peaked at 24 h post-exposure in both short- and long-duration CX exposure groups (Fig. 7).

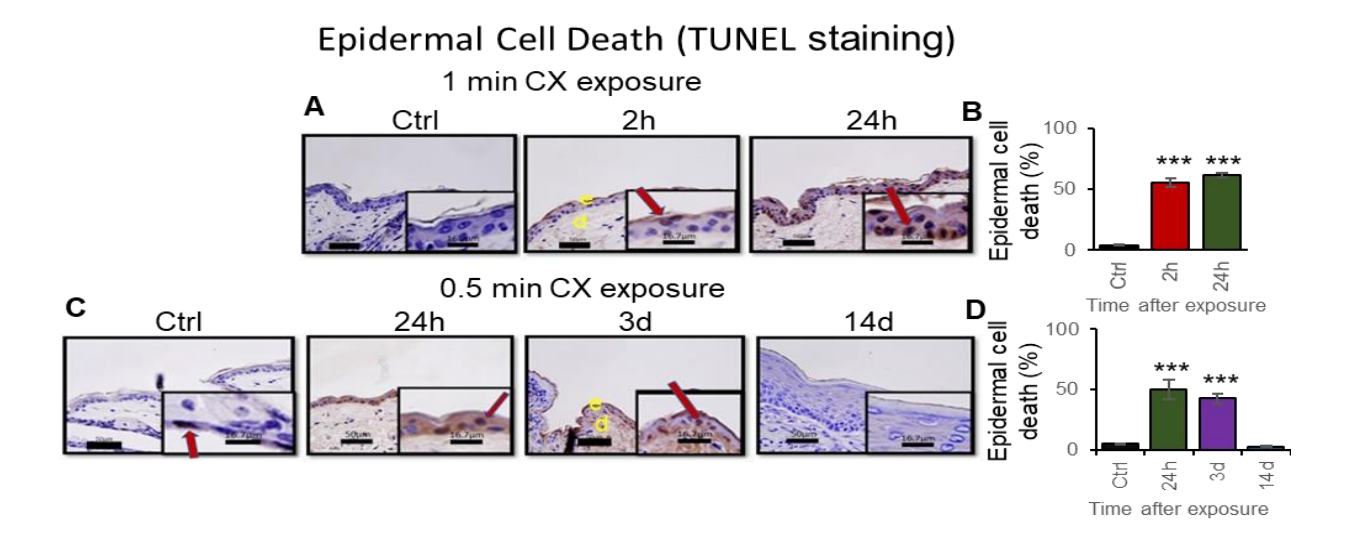


Figure 7: Effect of CX skin exposure on epidermal cell death in C57BL/6 mice. Representative pictures of TUNEL stained skin sections showing epidermal cell death (brown cells; red arrows); in male mice following (A) 1 min and (C) 0.5 min CX exposure and (B, D) their quantifications; e, epidermis; d, dermis; Data presented are mean \pm SEM (n=3). ***, p <0.001 compared to control.

CX skin exposure increased the expression of apoptotic cell death markers

As the TUNEL assay detects cell death by finding the nicks in DNA, we decided to evaluate the expression of cleaved caspase 3 and cleaved PARP1, which are considered the more specific apoptotic markers [28, 29] and are common in both the intrinsic and extrinsic apoptosis pathways, to confirm the apoptotic cell death. CX skin exposure for 1 min showed a significant increase of around 1.5-fold in cleaved caspase 3 at 2 h post-exposure (Fig. 8A). CX exposure for 0.5 min also resulted in around 2.2- and 3.8-fold increase in cleaved caspase 3 at 3- and 14-days post-exposure, respectively. Altogether, CX skin exposure caused an increase in cleaved caspase 3, which was significant at 3 days and 24 h post-exposure in the short and long-duration CX exposure groups, respectively, confirming the activation of apoptosis pathways (Fig 8A). CX skin exposure for 1 min caused a significant increase of more than 3-fold in cleaved PARP1 at 2 h that remained significant and more than 2.5-fold up to 24 h post-exposure (Fig. 8B). CX exposure for 0.5 min resulted in around 3.3- and 4.4-fold increases in cleaved PARP1 at 24 h and 3 days post-exposure, respectively, which was significantly higher than control mice at 3 days post-exposure (Fig. 8B). Overall, CX skin exposure caused an increase in apoptotic cell death which peaked at 2 h and 3 days post-exposure in the long- and short-duration CX exposure groups, respectively (Fig 8B). The fold change in the expression of these apoptotic markers in CX exposure shows that the expression levels of cleaved PARP1 increased at earlier time points as compared to cleaved caspase 3, indicating that cleaved caspase 3 might not detect apoptosis in the first days after CX exposure, while cleaved PARP1 does, and this might be due to the role of cleaved PARP1 as the early event after DNA damage [27] (Figs. 8A and B).

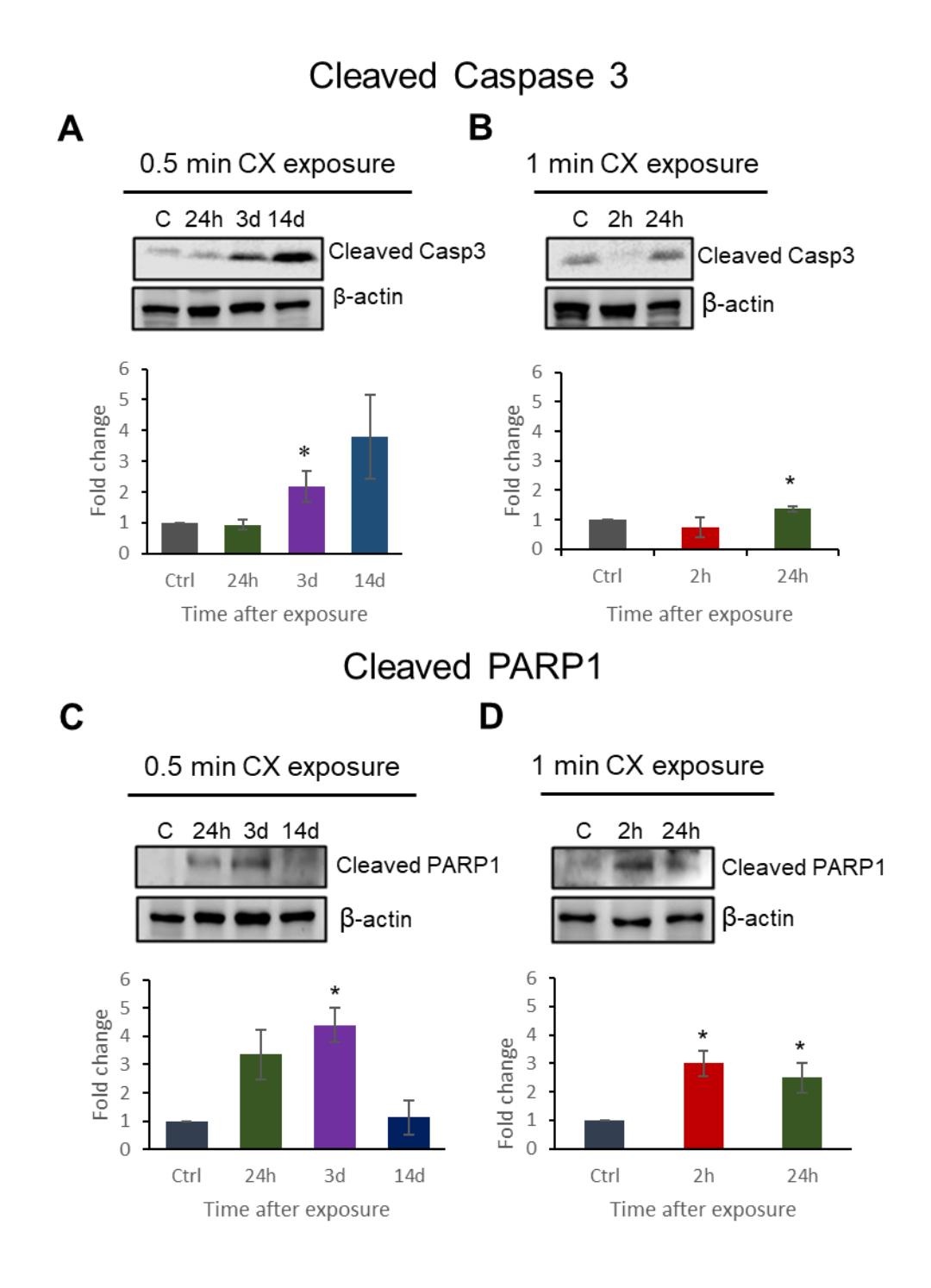


Figure 8: Effect of CX exposure on the expression of apoptosis molecular markers; cleaved caspase 3, and cleaved PARP1. Representative pictures of immunoblot on skin lysate showing increased apoptosis markers of (A) cleaved caspase 3 following 0.5 min CX exposure and its quantification; (B) cleaved caspase 3 following 1 min CX exposure and its quantification; (C) cleaved PARP1 following 0.5 min CX exposure and its quantification; and (D) cleaved PARP1 following 1 min CX exposure and its quantification; Data presented are mean ±SEM (n=3). *, p <0.05 compared to control.

CX skin exposure increased DNA damage markers

There are several pieces of evidence for widespread DNA damage after exposure to vesicating chemical agents like SM and LEW [13-15]. So, we studied the expression of the major DNA damage markers p53 ("Guardian of the genome"), phosphorylated p53 (ser 15), and phosphorylated H2A.X (ser 139) to determine the cause of cytotoxicity. CX skin exposure caused an increase in the specific DNA damage marker phosphorylated p53 which was significant at 2 h and 24 h post-exposure in the long-duration CX exposure group, and at 24 h and 3 days postexposure in the short-duration CX exposure group (Fig. 9A). CX skin exposure for 0.5 min resulted in around 2.5- and 5.6-fold increases in phosphorylated p53 at 24 h and 3 days post exposure, respectively, which were significantly higher than control mice (Fig. 9A). Also, CX skin exposure for 1 min caused a significant increase of 2.3-fold in phosphorylated p53 at 2 h post-exposure that remained significant and more than 2.5-fold up to 24 h post-exposure (Fig. 9A). In addition, the results showed a significant increase in total p53 accumulation. CX skin exposure for 1 min resulted in a significant increase of 1.9-fold at 2 h while CX skin exposure for 0.5 min caused a significant 3-fold increase at 24 h that remained significant and more than 3.3-fold up to 3 days post-exposure (Fig. 9B).

Phosphorylated H2A.X (ser 139) is the other important DNA damage marker that indicates double strand breaks [19] CX skin exposure for 1 min caused a significant increase of 3.4-fold in phosphorylated H2A.X at 2 h post-exposure compared to the control, which slightly decreased to 2.9-fold by 24 h post-exposure (Fig. 9C). Also, CX skin exposure for 0.5 min caused increases in the phosphorylated H2A.X at 24 h, and 3-day post-exposure; however, it was not statistically significant (Fig. 9C). The peak expression of total p53, phosphorylated p53, and phosphorylated H2A.X was at 3 days post-exposure in the short-duration CX exposure group. In the long-duration

CX exposure group, significant maximal expression of phosphorylated p53, total p53 and phosphorylated H2A.X were seen at 2 h post-exposure (Fig. 9). Together, CX skin exposure caused a significant increase in the DNA damage markers, implicating widespread DNA damage as the possible cause of apoptosis and cellular toxicity (Fig 9).

CX skin exposure increased oxidative DNA damage

The results of other researchers on vesicants, like NM and SM, suggest reactive ROS as the main contributor to DNA damage and apoptosis pathways stimulation [4, 22, 37]. Hence, we evaluated 8-OHdG, the main product of oxidative DNA damage [16] after CX exposure in C57BL/6 mice. CX skin exposure for 1 min and 0.5 min durations resulted in maximal increase in 8-OHdG positive cells (36%) at 2 h and 24 h post-exposure, respectively (Fig. 10). However, significant increases from 1 min and 0.5 min duration exposures were observed at 2 h and 3-day post-exposure, respectively (Fig. 10). Altogether, results showed a significant increase in 8-OHdG positive cells in C57BL/6 mice after short and long-duration CX skin exposure, indicating that oxidative stress plays a role in DNA damage after CX exposure, similar to the other vesicants (Fig 10).

CX skin exposure increased protein oxidation

Oxidative stress affects other macromolecules like lipids and proteins and contributes to cellular damage. Protein carbonyl groups are one of the most well-known markers of oxidative protein damage [17]. The results show that CX skin exposure for 0.5 min significantly increased protein carbonylation up to 2.3-fold at 24 h post-exposure (Fig. 11). However, CX skin exposure for 1 min increased protein carbonylation at 2 h compared to the control mice but it was not significant (Fig. 11).

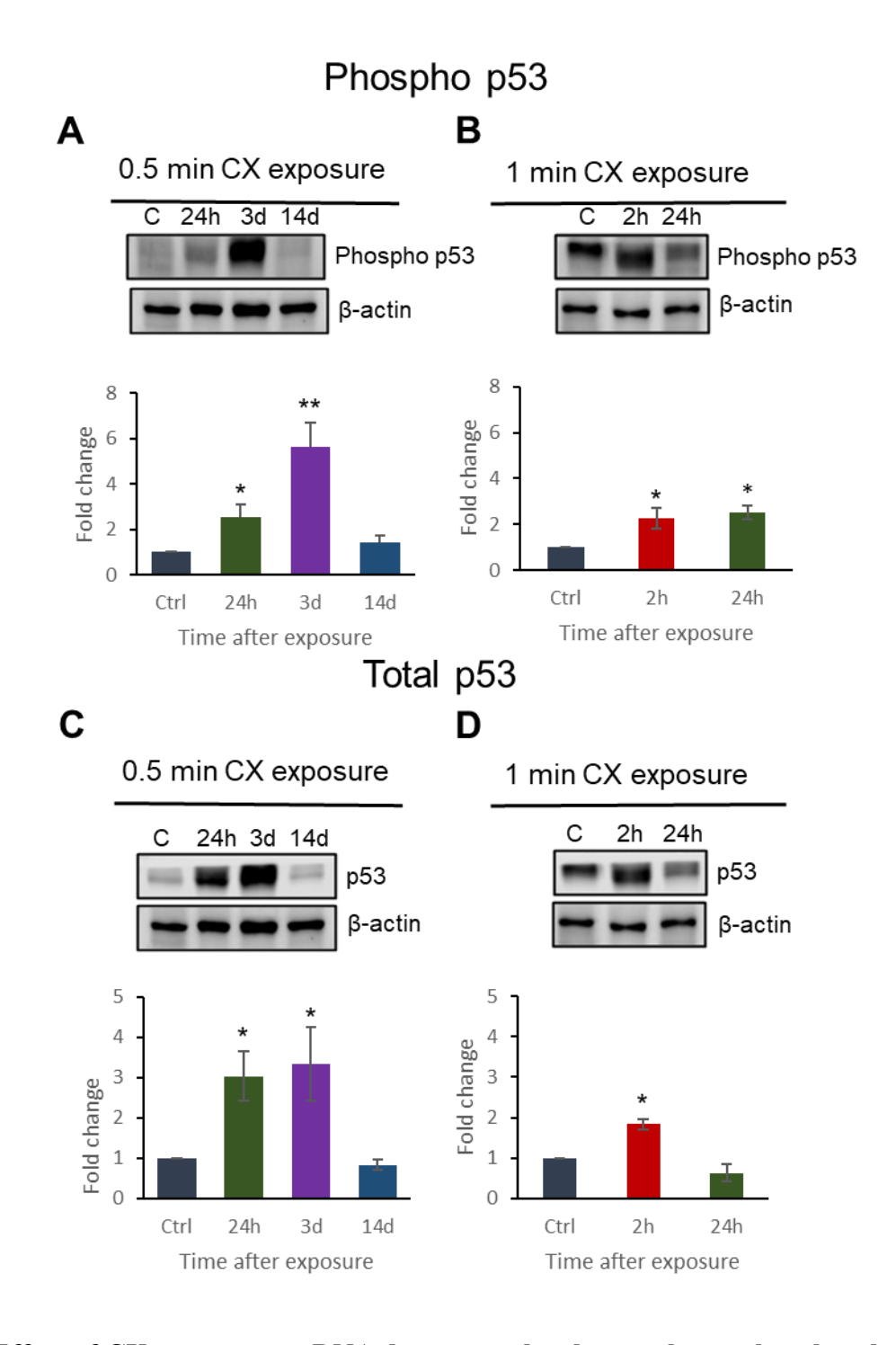
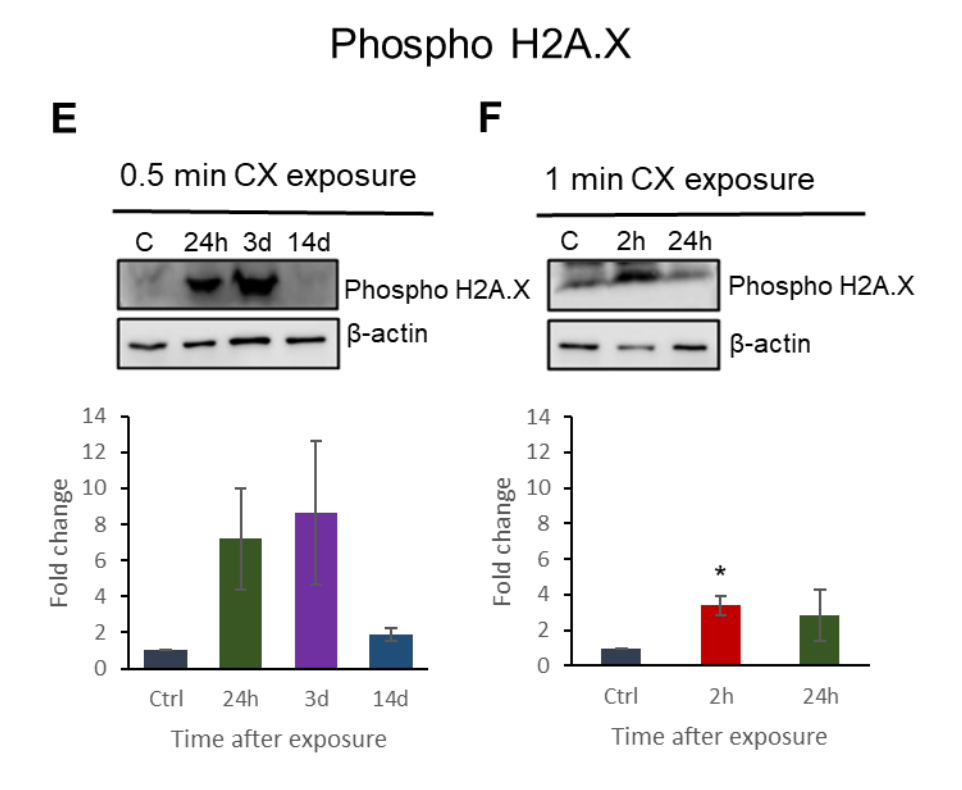


Figure 9: Effect of CX exposure on DNA damage molecular markers; phosphorylated p53, total p53 and phosphorylated H2A.X. Representative pictures of immunoblot on skin lysate showing increased DNA damage markers of (A) phosphorylated p53 (ser15) and (B) its quantification; (C) total p53 and (D) its quantification; (E) phosphorylated H2A.X (ser139) and (F) its quantification following 0.5 and 1 min CX exposure compared to the control group; Data presented are mean \pm SEM (n=3). *, p <0.05, **, p <0.01 compared to control.

Figure 9 (cont'd)



Largely, our results show increased oxidative protein damage after CX skin exposure, indicating a role for ROS in protein damage and widespread oxidative stress like what has been previously reported in other vesicants (Fig 11) [4, 22, 37].

CX skin exposure increased lipid peroxidation markers

Lipids are susceptible to oxidation and lipid peroxidation products like 4-HNE and MDA are potential biomarkers for oxidative stress in vivo[18, 31]. Hence, we investigated lipid peroxidation by evaluating 4-HNE to present more evidence for DNA damage by the effects of ROS on lipids and confirm widespread oxidative damage upon CX exposure. CX skin exposure for 0.5 min started with an increase of 4.3 folds lipid peroxidation after 24 h of CX exposure and reached a significant increase of 5.7-fold at 3 days post-exposure (Fig. 12). CX skin exposure for 1 min caused an increase of 2.6- and 1.9- fold at 2 h and 24 h, respectively. The increases in lipid

peroxidation confirmed the presence of oxidative stress, too. Altogether, our results showed a significant increase in lipid peroxidation in a time-dependent manner up to 3 days after 0.5 min CX exposure.

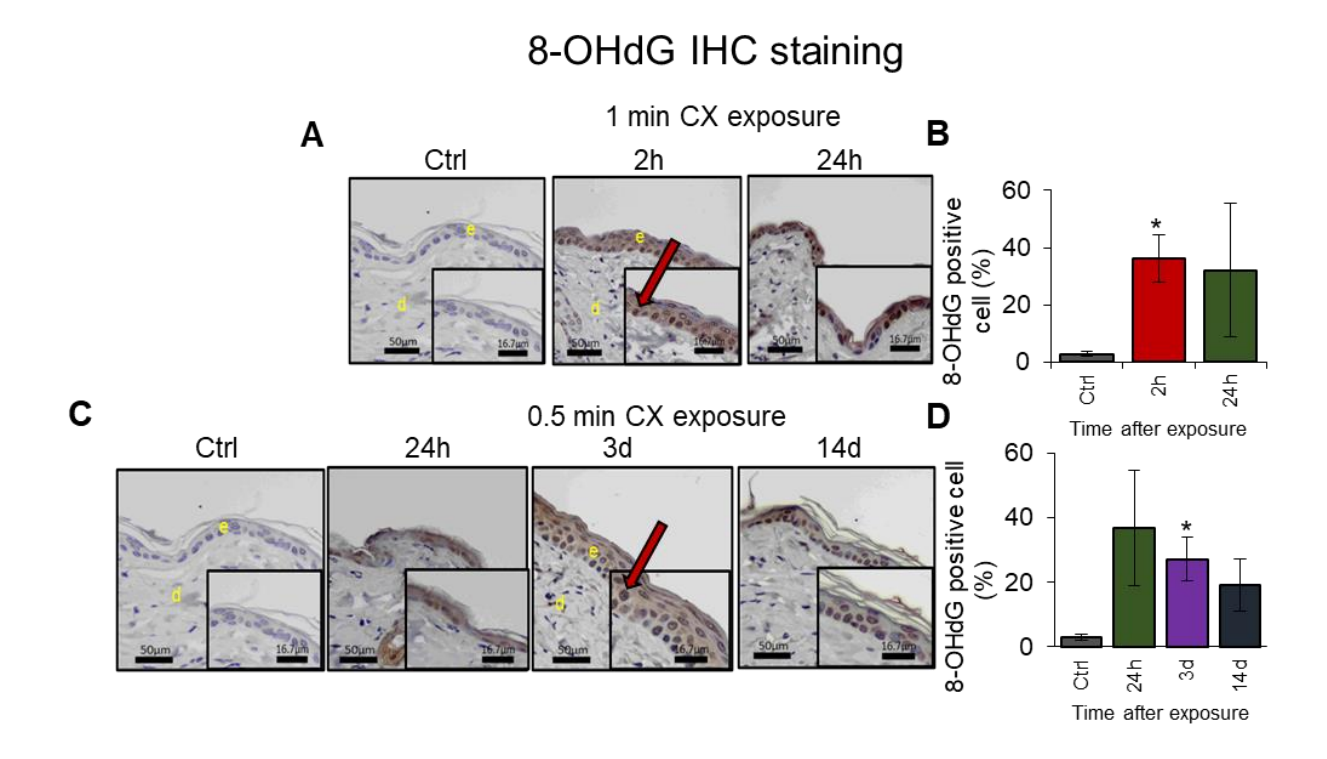


Figure 10: Effect of CX exposure on oxidative DNA damage in male C57BL/6 mice. Representative pictures of Immunohistochemistry (IHC) stained skin sections using anti-8-OHdG antibody showing oxidative DNA damage (brown cells; Red arrows); in male mice following (A) 1 min CX exposure and (B) its quantification, (C) 0.5 min CX exposure, and (D) its quantification; e, epidermis; d, dermis; Data presented are mean ±SEM (n=3). *, p <0.05 compared to control.

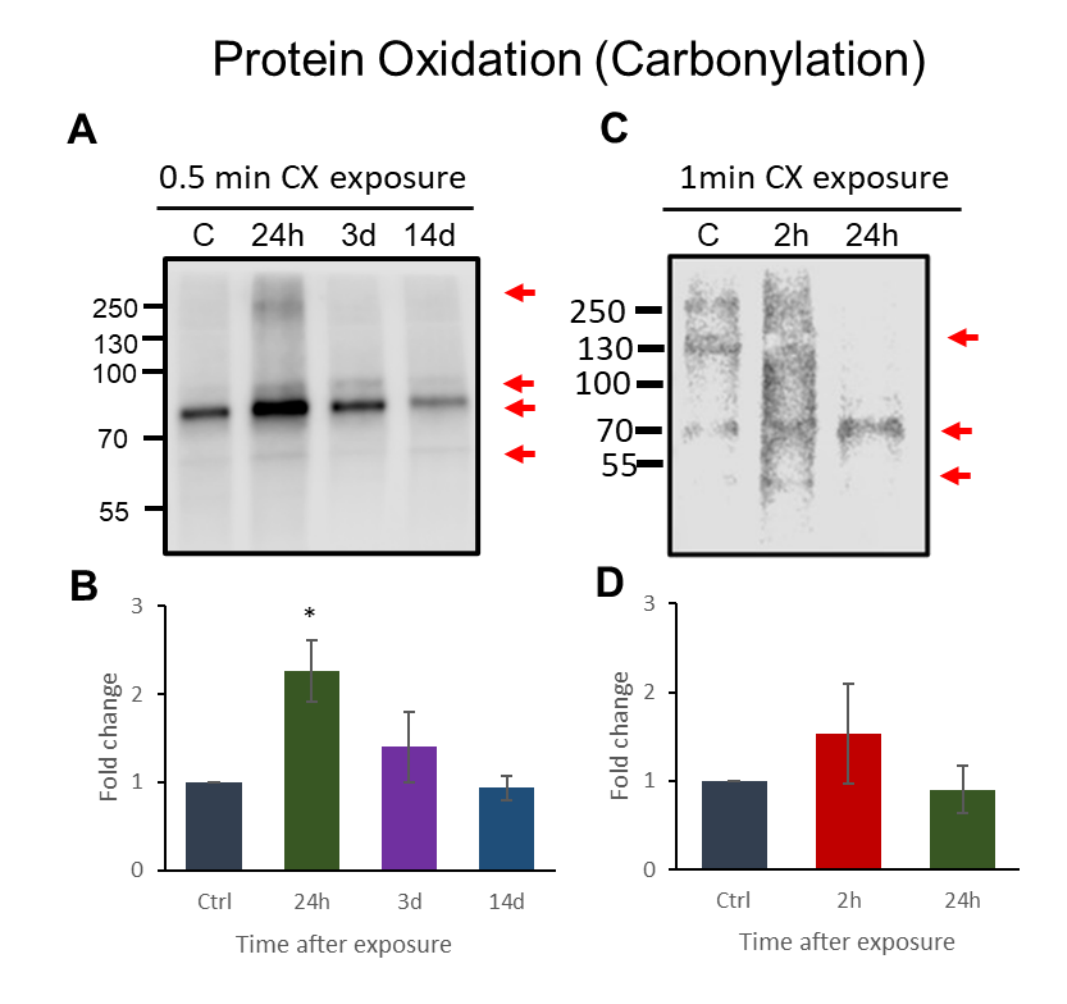


Figure 11: Effect of CX skin exposure on Protein Oxidation (Carbonylation) in the male C57BL/6 mice. Carbonyl groups in the protein side chain were derivatized with 2,4-Dinitrophenylhydrazine (DNPH) to DNP hydrazone and then were detected using anti-DNP antibody by immunoblotting. Entire lane density was utilized for fold change analysis. Representative pictures of immunoblot on skin lysate showing increased Protein Oxidation (Red arrows) following (A) 0.5 min CX exposure and (B) its quantification; and (C) 1 min CX exposure and (D) its quantification; Data presented are mean ±SEM (n=3). *, p <0.05 compared to control.

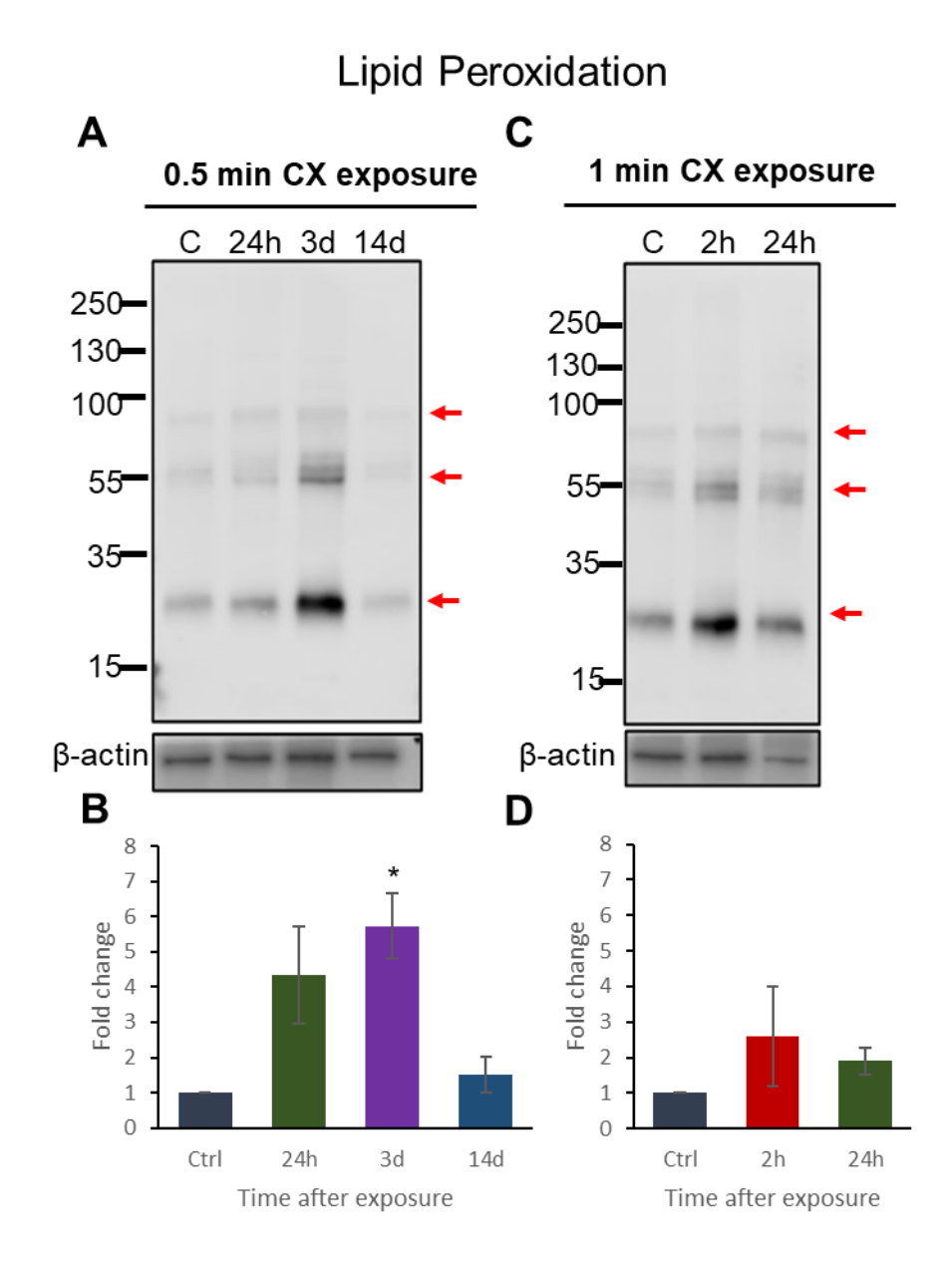


Figure 12: Effect of CX skin exposure on lipid peroxidation in the male C57BL/6 mice. 4-HNE adduct as the lipid peroxidation marker was detected using the anti-4-HNE antibody by immunoblotting. Representative pictures of immunoblot on skin lysate showing increased lipid peroxidation (Red arrows) following (A) 0.5 min CX exposure and (B) its quantification; and (C) 1 min CX exposure and (D) its quantification; Data presented are mean \pm SEM (n=3). *, p <0.05 compared to control.

CHAPTER 3: DISCUSSION

3.1 Discussion

The use of chemical warfare agents has a long history but only since WWI has it posed a serious threat to both soldiers and civilians. During WWI, Germany and some other countries used chlorine gas, phosgene, SM, and LEW which altogether resulted in a recorded 1.2 million casualties and over 100,000 deaths [50]. Also, during the 20th century, probably 70 distinct chemicals or chemical combinations have been utilized or stored for CW purposes [1].

CX is categorized as a vesicant, but it also causes urticaria, unlike the other members of the vesicant class which mainly cause blisters. It is more potent than other vesicating agents and is considered an emerging chemical threat; however, its mechanism of action, which is unknown, needs to be elucidated [11]. Despite it being produced by Germany during WWI and developed and stockpiled by Germany and Russia, there have been no reports of its usage, no comprehensive pathophysiological study, and no therapy or antidote [11].

Because it is highly toxic, the use of CX for laboratory animal exposure or cell culture is not permitted in routine laboratory settings, and since there are no surrogates for CX like those available for SM [2-Chloroethyl ethyl sulfide (CEES); NM] or LEW (Phenylarsine oxide, PAO), studies are accompanied with limitations. Animal exposures need to be performed at approved companies with appropriate safety measures in place like MRIGlobal, Kansas City, MO, and study samples are shipped to the university labs for further analysis [37, 51].

The first pilot study on CX skin exposure by Tewari-Singh et al. published in 2017 showed skin lesions of urticaria, erythema, necrosis, edema, and blanching of exposed skin with an erythematous ring and the involvement of DNA damage, apoptosis, and inflammation pathways. However, this study was limited to just acute exposure in hairless mice and the skin samples from

one-time point of 8 h after CX exposure were analyzed [10]. The goal of my current study was to examine the DNA damage and oxidative stress-related damaging effects of CX at two exposure durations to elucidate the mechanism of CX toxicity in haired mice. To elucidate the mechanism of action of CX, one of the first steps was to examine the effects of acute lethal and non-lethal CX exposures and the development and progression of toxic effects over time. Therefore, we designed this study in the C57BL/6 mouse strain to investigate the acute effects of CX and injury progression and establish biomarkers that can be used for mechanistic studies on genetically modified mice available in this genetic background.

However, since the final goal of our studies is to identify therapeutic targets and develop treatments for human toxicity after CX exposure, using animal model with skin that resembles human skin is a more appropriate injury model. Since pig is the best model for human skin exposure, exposure to the pig skin should be considered in the next steps, after mechanistic studies, for confirming the mice model results [52].

Our previous pilot study (unpublished) with different doses of CX showed that exposure to $10~\mu l$ of CX for 1 minute killed 50% of the mice, while there was no mortality in the group given it for 0.5 minutes. Therefore, we considered 1 min as acute lethal contact with mortality and 0.5 min as acute-nonlethal CX exposure that enables us to follow the CX lesions over time. To follow the toxic changes after CX exposure, we chose the study time points according to changes in the macroscopic skin lesions observed after CX exposure in the pilot study. Hence, the dorsal skin of mice was exposed to CX for short (acute non-lethal) and long (acute lethal) periods; 0.5 and 1 min, respectively, and skin samples were collected at different time points post-exposure to study the injury progression in terms of clinical, biological, and molecular effects.

The results of this study show a significant increase in apoptotic cell death in the epidermal cells within a very short time of 2 h after CX exposure, which has been reported with other vesicants like NM, SM, and LEW [15, 53]. Studies with LEW have shown extensive apoptosis in the epidermal keratinocytes and cutaneous exposure to PAO, a less toxic surrogate of LEW, in Ptch1+/-/SKH-1 mouse skin (Ptch1+/-/SKH-1 is a mice model for development of Basal Cell Carcinoma and also has shown highly sensitive murine model to demonstrate the toxic manifestations of environmental agents on the skin; Ptch1 is a tumor suppressor gene) resulted in apoptosis at 4 h post-exposure beginning in hair follicles, spreading to the inter hair follicle epithelial cells later near 16 h post-exposure [51, 54]. With mustard vesicant NM, skin epidermal cell apoptosis was observed to increase in different studies. NM exposure caused a significant increase at 12, 24, 72, and 120 h post exposure while the peak of apoptosis was observed at 12 h and 24 h post exposure in SKH-1 and C57BL/6 mice, respectively [49, 53]. Also, exposure to a less toxic analog of SM, CEES, showed a significant increase at 6 h post exposure while the peak of apoptosis was observed at 72 h post exposure [46]. Together, our results with CX are comparable with other vesicants showing apoptosis as one of the pathologic features after exposure to vesicant agents; however, these cytotoxic effects were more rapid with CX than reported for other vesicants. We focused on analyzing the apoptotic cell death pathway because it involves programmed cell death mechanism that can be targeted to reverse cell toxicity, which is our longterm goal to find an effective antidote for the treatment of CX-induced injury.

TUNEL assay detects nicks in DNA and marks the cells, allowing for the measurement of apoptosis. Signaling pathways leading to apoptosis could be considered as the therapeutic target, which have been tested in other vesicants like SM and NM [49, 55]. In response to external inputs, the protein kinase B-Raf, a component of the Ras/Raf/MEK/ERK signaling pathway, governs cell

proliferation, differentiation, and migration. Raf kinase family inhibitor vemurafenib in a study caused a decrease in SM-induced epidermal apoptosis [49]. Another study with flavonoid silibinin, with targets pathways associated with DNA damage, apoptosis, and oxidative stress, showed strong efficacy in ameliorating NM-induced skin injuries [19, 49, 55]. Targeting specific apoptotic regulators involves a variety of innovative techniques, including antisense and gene therapy, recombinant biologics, and traditional chemical and combinatorial chemistry [56, 57]. To confirm the mechanism of apoptosis, we measured changes in two specific apoptotic markers: cleaved caspase 3 and cleaved PARP1. These two markers are activated in both intrinsic and extrinsic apoptosis pathways [28, 29]. Our results indicate a CX-induced increase in both the apoptotic markers but an enhanced expression of PARP1 at the earlier time points post CX exposure indicating that possibly it is a more sensitive marker of CX exposure.

Previous studies have shown that DNA damage and activation of p53 are initial triggers that cause apoptosis in the skin epidermal cells upon NM and SM exposure [41, 58]. Genotoxicity can lead to cellular toxicity and trigger the DNA damage response (DDR) to protect the cells. DNA damage sensed by ATM, ATR and DNA-PK recruits phosphorylated H2AX and p53 to sites of DNA lesions to repair the DNA [24]. Excessive DNA modification can overwhelm the cell's DNA repair capabilities, leading to DNA breaks and apoptosis. So, increased DNA damage and the activation of program cell death pathways could be a possible cause of apoptosis [59]. The results of this study show a significant increase in total p53, phosphorylated p53 and H2A.X in the skin tissue within 2 h of CX exposure, indicating strong activation of the DNA damage response. Since the main role of H2A.X in DNA repair is increasing access to DNA repair proteins, it is a good marker to indicate the initiation of DDR and its increase together with the increase of p53 could indicate the activation of DDR and DNA repair pathways simultaneously [58]. Studies on vesicants like

mustard agents have shown that DNA damage is involved in cellular toxicity of these agents, and the activation of p53 as well as H2A.X are key early events [14]. However, determining the mechanisms of DNA damage and repair is still underway because there are numerous pathways that cause DNA damage, and their induction frequently depends on time and/or cell cycle phase as well as concentration and tissue distribution of toxic agent, if studies are conducted *in vivo* [58]. The results of our study on DNA damage markers in the skin of C57BL/6 mice after both shortand long-duration CX exposures suggests that CX skin toxicity involves p53 and H2A.X related pathways that could be parallel to the other vesicants and related pathways may possibly be potential therapeutic targets.

It is not known whether CX possesses nucleophilic and alkylating properties that cause CX-related DNA damage or if it is the increased oxidative stress that is harmful for DNA and the other macromolecules, both of which have been reported as mechanisms of mustard vesicating agents-induced skin injury [4, 11, 26, 60]. To investigate the cause of DNA damage and apoptosis in the skin toxicity from CX exposure, we further evaluated the oxidative stress related damage to biomolecules, including DNA, in CX-exposed mice. The results showed an increase in oxidative DNA damage, protein oxidation (carbonylation), and lipid peroxidation in both the acute lethal and non-lethal exposure groups, confirming extensive oxidative stress after CX exposure. Since CX is an urticant and results from other studies in our laboratory have shown that mast cell degranulation could play an important role in the CX-related skin inflammatory response and toxicity, DNA damage could be a direct effect of oxidative stress or, via the oxidative stress from an inflammatory response following mast cell activation, or both [10]. This is being further analyzed in our laboratory using mast cell-deficient mice to better determine therapeutic targets. Also, at 24 h post exposure, an exposure duration- dependent effect of 0.5 and 1 min CX was not

observed in all the studied toxicity markers, which could be due to several reasons and needs to be further investigated. It is well recognized that oxidative stress plays an important role in alkylating mustard vesicating agents-induced skin toxicity, and many drug candidates are being tested that can target oxidative stress pathways to reduce tissue injury [36]. This study established the DNA damage and apoptosis after CX exposure and indicated that CX skin exposure could lead to oxidative stress and further damaging response similar to other vesicants; therefore, elucidation of oxidative stress related pathways to identify potential therapeutic targets is warranted (Fig. 13).

3.2 Future directions

- Based on the detection of some gender-related differences in our preliminary studies, we want to determine any gender-related differences in CX-induced DNA damage and oxidative stress-induced toxicity by comparing the data from this study in male mice with the female C57BL/6 mice.
- Based on the results herein indicating damage to proteins and lipids, we would like to
 follow up on dissecting the related pathways and evaluate them for finding new
 therapeutic targets.
- By using N-acetylcysteine (NAC) as a pro-drug for the synthesis of antioxidant glutathione (GSH), which logically should decrease the oxidative stress and consequently CX toxicity, we can further confirm the contribution of oxidative stress from CX toxicity [61, 62].
- In our previous studies, exposure to urticant CX, has been shown to cause a more robust increase in mast cell degranulation, histamine release and an inflammatory response (inflammation is one of the sources of oxidative stress) as compared to mustard vesicating agents (Fig 14) [63]. This study shows that CX exposure resulted in

oxidative stress, damage to DNA and other macromolecules. This could be directly via oxidative stress or indirectly via oxidative stress generated by an inflammatory response mainly due to mast cell degranulation, or both (Fig. 15) [31]. Altogether, since mast cells are the main players in hypersensitivity type 1 which can manifest as urticaria, the possible role of mast cells in CX induced inflammation and oxidative stress leading to cytotoxicity is being further investigated using mast cell knockout mice.

• Since there is the possibility that CX induces inflammation and injury involving additional mechanisms, RNA-seq and Nano string techniques will be further employed to aid in elucidating CX-induced signaling pathways and identify therapeutic targets to treat CX skin injuries.

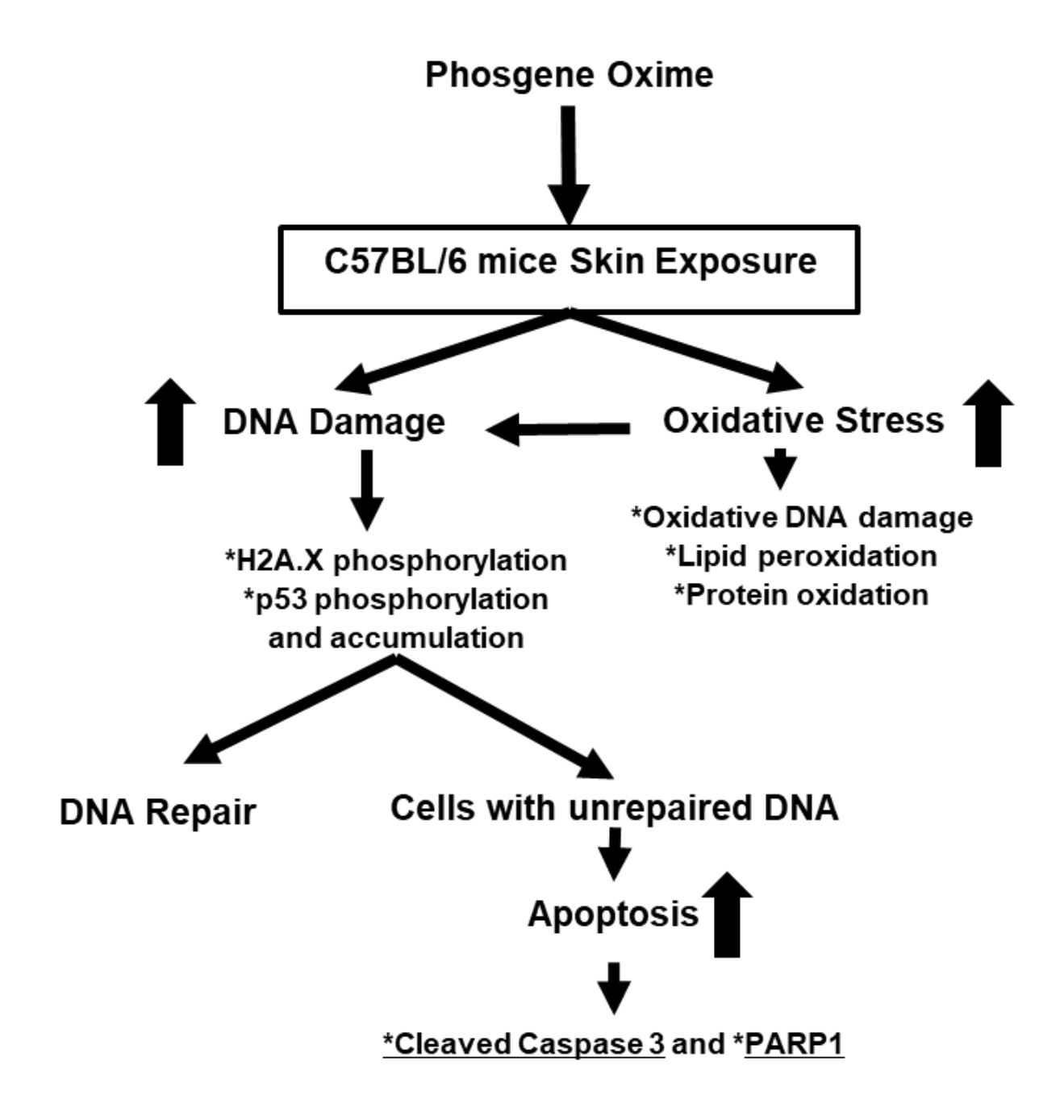


Figure 13: Summary figure. CX exposure to skin of C57BL/6 mice increased DNA damage detected by significant increases in phosphorylated p53, total p53 and phosphorylated H2A.X. Cells with damaged DNA, which is not repaired, enter to apoptotic pathway which was detected in CX exposed cells where elevated levels of cleaved caspase 3 and PARP1 were observed as compared to control skin cells. Also, CX skin exposure caused an increase in oxidative stress which was detected by increased levels of oxidative DNA damage, lipid peroxidation and protein carbonylation as compared to control. * Shows markers employed for the detection of oxidative stress, DNA damage and programmed cell death pathway.

Mast Cell Degranulation

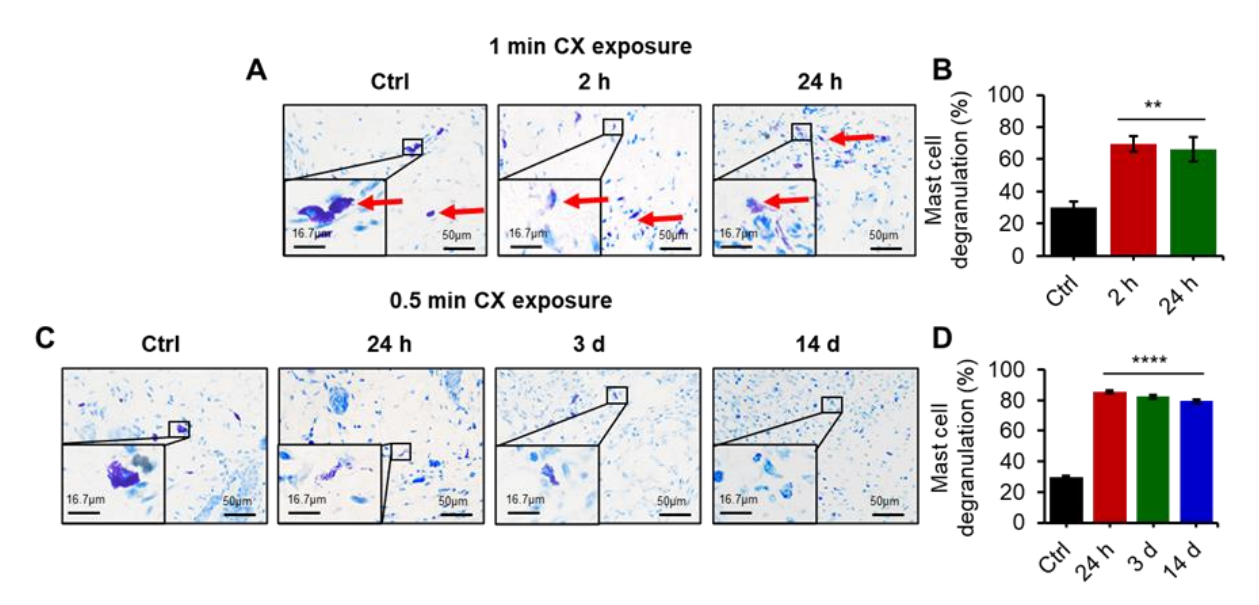


Figure 14: Effect of CX skin exposure on dermal mast cell degranulation in male C57BL/6 mice. Representative pictures of toluidine blue-stained skin sections showing mast cell degranulation (purple cells; red arrows) following (A) 1 min CX exposure and (B) its quantification, and (C) 0.5 min CX exposure and (D)its quantification in male C57BL/6 mice. Data presented are mean \pm SEM (n=3-5). **, p <0.01; ****, p <0.0001 compared to control group.

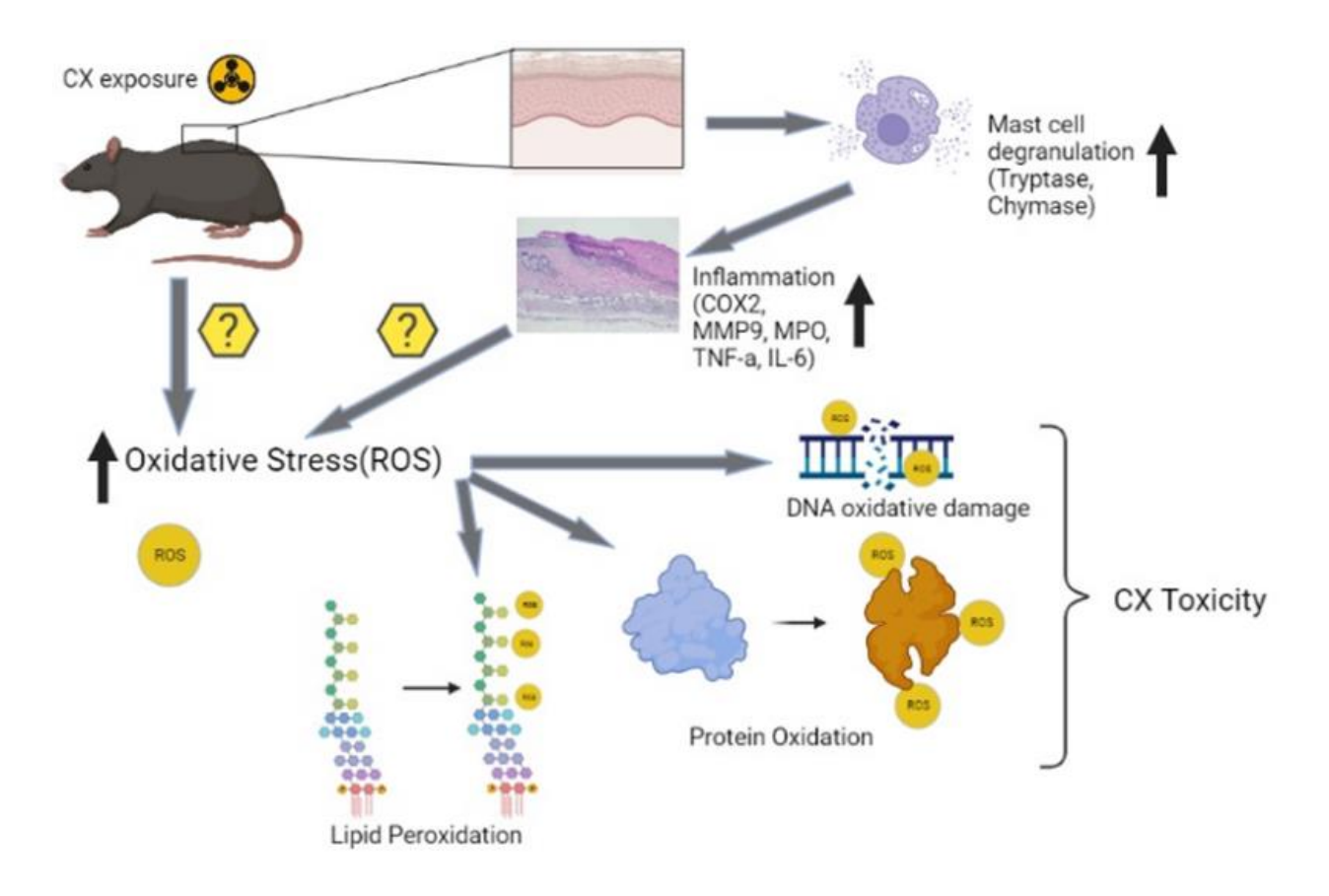


Figure 15: Schematic presentation of the possible role of mast cells and inflammation in CX-related oxidative stress and toxicity (further investigation). CX has been shown to increase oxidative stress, which can directly cause oxidative damage to DNA, protein, and lipids and toxicity. Also, the high degree of mast cell degranulation with urticaria-like lesions indicates the involvement of mast cells in CX toxicity by increasing inflammation and oxidative stress, which needs further investigation. COX2, Cyclooxygenase-2; MMP9, Matrix metallopeptidase 9; MPO, Myeloperoxidase, TNF-a, Tumor necrosis factor-alpha; IL6, Interleukin 6; ROS, Reactive oxygen species.

BIBLIOGRAPHY

- 1. Ganesan, K., S.K. Raza, and R. Vijayaraghavan, *Chemical warfare agents*. J Pharm Bioallied Sci, 2010. **2**(3): p. 166-78.
- 2. Kuca, K. and M. Pohanka, *Chemical warfare agents*. EXS, 2010. **100**: p. 543-58.
- 3. Dacre, J.C. and M. Goldman, *Toxicology and pharmacology of the chemical warfare agent sulfur mustard*. Pharmacol Rev, 1996. **48**(2): p. 289-326.
- 4. Goswami, D.G., R. Agarwal, and N. Tewari-Singh, *Phosgene oxime: Injury and associated mechanisms compared to vesicating agents sulfur mustard and lewisite.* Toxicol Lett, 2018. **293**: p. 112-119.
- 5. Tucker, J.B.I.F., War of nerves: chemical warfare from world War I to Al-Qaeda 2006.
- 6. Pitschmann, V., *Overall view of chemical and biochemical weapons*. Toxins, 2014. **6**(6): p. 1761-1784.
- 7. Bowen, W., J.W. Knopf, and M. Moran, *The Obama Administration and Syrian Chemical Weapons: Deterrence, Compellence, and the Limits of the "Resolve plus Bombs" Formula*. Security Studies, 2020. **29**(5): p. 797-831.
- 8. Chauhan, S., et al., *Chemical warfare agents*. Environmental Toxicology and Pharmacology, 2008. **26**(2): p. 113-122.
- 9. Patočka, J. and K. Kuča, *PHOSGENE OXIME–FORGOTEN CHEMICAL WEAPON*. Military Medical Science Letters, 2011. **80**: p. 38-41.
- 10. Tewari-Singh, N., et al., *Cutaneous exposure to vesicant phosgene oxime: Acute effects on the skin and systemic toxicity.* Toxicology and applied pharmacology, 2017. **317**: p. 25-32.
- 11. Tewari-Singh, N., *Phosgene oxime*, in *Handbook of toxicology of chemical warfare agents*. 2020, Elsevier. p. 197-202.
- 12. Augerson, W.S., A review of the scientific literature as it pertains to Gulf War illnesses. 2000.
- 13. Goswami, D.G., et al., Nitrogen mustard-induced corneal injury involves DNA damage and pathways related to inflammation, epithelial-stromal separation and neovascularization. Cornea, 2016. **35**(2): p. 257.
- 14. Inturi, S., et al., *Mechanisms of sulfur mustard analog 2-chloroethyl ethyl sulfide-induced DNA damage in skin epidermal cells and fibroblasts*. Free Radical Biology and Medicine, 2011. **51**(12): p. 2272-2280.

- 15. Srivastava, R.K., et al., *Cutaneous exposure to lewisite causes acute kidney injury by invoking DNA damage and autophagic response*. American Journal of Physiology-Renal Physiology, 2018. **314**(6): p. F1166-F1176.
- 16. Jan, Y.-H., et al., Sulfur mustard analog mechlorethamine (Bis (2-chloroethyl) methylamine) modulates cell cycle progression via the DNA damage response in human lung epithelial A549 cells. Chemical research in toxicology, 2019. **32**(6): p. 1123-1133.
- 17. Broude, E.V., et al., *p21* (*CDKN1A*) is a negative regulator of *p53* stability. Cell Cycle, 2007. **6**(12): p. 1467-1470.
- 18. Meek, D.W., *The p53 response to DNA damage*. DNA repair, 2004. **3**(8-9): p. 1049-1056.
- 19. Tewari-Singh, N. and R. Agarwal, *Mustard vesicating agent–induced toxicity in the skin tissue and silibinin as a potential countermeasure*. Annals of the New York Academy of Sciences, 2016. **1374**(1): p. 184-192.
- 20. Agarwal, A., et al., *Potential biological role of poly (ADP-ribose) polymerase (PARP) in male gametes.* Reproductive Biology and Endocrinology, 2009. **7**: p. 1-20.
- 21. De Zio, D., V. Cianfanelli, and F. Cecconi, *New insights into the link between DNA damage and apoptosis*. Antioxidants & redox signaling, 2013. **19**(6): p. 559-571.
- 22. Beigi Harchegani, A., et al., *Role of oxidative stress and antioxidant therapy in acute and chronic phases of sulfur mustard injuries: a review.* Cutaneous and ocular toxicology, 2019. **38**(1): p. 9-17.
- 23. Clewell, R.A., et al., *Profiling dose-dependent activation of p53-mediated signaling pathways by chemicals with distinct mechanisms of DNA damage*. Toxicological sciences, 2014. **142**(1): p. 56-73.
- 24. Baran, K., D. Rodriguez, and D. Green, *The DNA damage response mediates apoptosis and tumor suppression*. Cell Death: Mechanism and Disease, 2014: p. 135-165.
- 25. Vadivel Gnanasundram, S., et al., *p53 mRNA metabolism links with the DNA damage response*. Genes, 2021. **12**(9): p. 1446.
- 26. Ray, R., et al., Sulfur mustard induces apoptosis in lung epithelial cells via a caspase amplification loop. Toxicology, 2010. **271**(3): p. 94-99.
- 27. Mashimo, M., et al., *The 89-kDa PARP1 cleavage fragment serves as a cytoplasmic PAR carrier to induce AIF-mediated apoptosis.* Journal of Biological Chemistry, 2021. **296**.
- 28. Choudhary, G.S., S. Al-Harbi, and A. Almasan, *Caspase-3 activation is a critical determinant of genotoxic stress-induced apoptosis*. Apoptosis and Cancer: Methods and Protocols, 2015: p. 1-9.

- 29. Qvarnström, O., et al., γ*H2AX and cleaved PARP-1 as apoptotic markers in irradiated breast cancer BT474 cellular spheroids.* International journal of oncology, 2009. **35**(1): p. 41-47.
- 30. Borna, H., et al., A review on proteomics analysis to reveal biological pathways and predictive proteins in sulfur mustard exposed patients: roles of inflammation and oxidative stress. Inhalation toxicology, 2019. **31**(1): p. 3-11.
- 31. Hennino, A., et al., *Pathophysiology of urticaria*. Clinical reviews in allergy & immunology, 2006. **30**: p. 3-11.
- 32. Sena, L.A. and N.S. Chandel, *Physiological roles of mitochondrial reactive oxygen species*. Molecular cell, 2012. **48**(2): p. 158-167.
- 33. Chelombitko, M., et al., *Role of reactive oxygen species in mast cell degranulation*. Biochemistry (Moscow), 2016. **81**: p. 1564-1577.
- 34. Zeng, M.Y., et al., *The roles of NADPH oxidase in modulating neutrophil effector responses*. Molecular oral microbiology, 2019. **34**(2): p. 27-38.
- 35. Ranneh, Y., et al., Crosstalk between reactive oxygen species and pro-inflammatory markers in developing various chronic diseases: a review. Applied Biological Chemistry, 2017. **60**(3): p. 327-338.
- 36. Laskin, J.D., et al., *Oxidants and antioxidants in sulfur mustard–induced injury*. Annals of the New York Academy of Sciences, 2010. **1203**(1): p. 92-100.
- 37. Pal, A., et al., Sulfur mustard analog induces oxidative stress and activates signaling cascades in the skin of SKH-1 hairless mice. Free Radical Biology and Medicine, 2009. **47**(11): p. 1640-1651.
- 38. Barzilai, A. and K.-I. Yamamoto, *DNA damage responses to oxidative stress*. DNA repair, 2004. **3**(8-9): p. 1109-1115.
- 39. Aubrey, B.J., et al., *How does p53 induce apoptosis and how does this relate to p53-mediated tumour suppression?* Cell death & differentiation, 2018. **25**(1): p. 104-113.
- 40. Cadet, J., et al., Formation and repair of oxidatively generated damage in cellular DNA. Free Radical Biology and Medicine, 2017. **107**: p. 13-34.
- 41. Kumar, D., et al., Nitrogen mustard exposure of murine skin induces DNA damage, oxidative stress and activation of MAPK/Akt-AP1 pathway leading to induction of inflammatory and proteolytic mediators. Toxicology letters, 2015. 235(3): p. 161-171.

- 42. Mantena, S.K. and S.K. Katiyar, *Grape seed proanthocyanidins inhibit UV-radiation-induced oxidative stress and activation of MAPK and NF-κB signaling in human epidermal keratinocytes*. Free Radical Biology and Medicine, 2006. **40**(9): p. 1603-1614.
- 43. Levine, R.L., et al., *Determination of carbonyl groups in oxidized proteins*. Stress Response: Methods and Protocols, 2000: p. 15-24.
- 44. Stadtman, E.R., *Protein oxidation in aging and age-related diseases*. Annals of the new York Academy of Sciences, 2001. **928**(1): p. 22-38.
- 45. Tewari-Singh, N., et al., *Inflammatory Biomarkers of Sulfur Mustard Analog 2-Chloroethyl Ethyl Sulfide–Induced Skin Injury in SKH-1 Hairless Mice.* Toxicological sciences, 2009. **108**(1): p. 194-206.
- 46. Jain, A.K., et al., *Histopathological and immunohistochemical evaluation of nitrogen mustard-induced cutaneous effects in SKH-1 hairless and C57BL/6 mice*. Experimental and Toxicologic Pathology, 2014. **66**(2-3): p. 129-138.
- 47. Inturi, S., et al., *Activation of DNA damage repair pathways in response to nitrogen mustard-induced DNA damage and toxicity in skin keratinocytes.* Mutation Research/Fundamental and Molecular Mechanisms of Mutagenesis, 2014. **763**: p. 53-63.
- 48. Valavanidis, A., T. Vlachogianni, and C. Fiotakis, 8-hydroxy-2'-deoxyguanosine (8-OHdG): a critical biomarker of oxidative stress and carcinogenesis. Journal of environmental science and health Part C, 2009. 27(2): p. 120-139.
- 49. Xiao, Z., et al., *B-Raf inhibitor vemurafenib counteracts sulfur mustard-induced epidermal impairment through MAPK/ERK signaling*. Drug and Chemical Toxicology, 2022: p. 1-10.
- 50. Johnson, N.H., J.C. Larsen, and E.C. Meek, *Historical perspective of chemical warfare agents*, in *Handbook of toxicology of chemical warfare agents*. 2020, Elsevier. p. 17-26.
- 51. Li, C., et al., Molecular mechanism underlying pathogenesis of lewisite-induced cutaneous blistering and inflammation: chemical chaperones as potential novel antidotes. The American journal of pathology, 2016. **186**(10): p. 2637-2649.
- 52. Sullivan, T.P., et al., *The pig as a model for human wound healing*. Wound repair and regeneration, 2001. **9**(2): p. 66-76.
- 53. Inturi, S., et al., Absence of a p53 allele delays nitrogen mustard-induced early apoptosis and inflammation of murine skin. Toxicology, 2013. **311**(3): p. 184-190.
- 54. Srivastava, R.K., et al., *Defining cutaneous molecular pathobiology of arsenicals using phenylarsine oxide as a prototype*. Scientific reports, 2016. **6**(1): p. 34865.

- 55. Jain, A.K., et al., Flavanone silibinin treatment attenuates nitrogen mustard-induced toxic effects in mouse skin. Toxicology and applied pharmacology, 2015. **285**(1): p. 71-78.
- 56. Fischer, U. and K. Schulze-Osthoff, *Apoptosis-based therapies and drug targets*. Cell Death & Differentiation, 2005. **12**(1): p. 942-961.
- 57. Geske, F., et al., *Early stages of p53-induced apoptosis are reversible*. Cell Death & Differentiation, 2001. **8**(2): p. 182-191.
- 58. Jan, Y.-H., et al., *DNA damage signaling in the cellular responses to mustard vesicants.* Toxicology letters, 2020. **326**: p. 78-82.
- 59. Roos, W.P. and B. Kaina, *DNA damage-induced cell death: from specific DNA lesions to the DNA damage response and apoptosis.* Cancer letters, 2013. **332**(2): p. 237-248.
- 60. Nair, A., et al., *Toxic blister agents: Chemistry, mode of their action and effective treatment strategies.* Chemico-Biological Interactions, 2021. **350**: p. 109654.
- 61. Tewari-Singh, N., et al., *Efficacy of glutathione in ameliorating sulfur mustard analog-induced toxicity in cultured skin epidermal cells and in SKH-1 mouse skin in vivo*. Journal of Pharmacology and Experimental Therapeutics, 2011. **336**(2): p. 450-459.
- 62. Wright, H., et al., *Investigation of the Nrf2 Pathway in Mitigating Nitrogen Mustard and Chloropicrin Induced Corneal Injury*. Investigative Ophthalmology & Visual Science, 2022. **63**(7): p. 3235–A0270-3235–A0270.
- 63. Cruz-Hernandez, A., et al., *Mast cells promote nitrogen mustard-mediated toxicity in the lung associated with proinflammatory cytokine and bioactive lipid mediator production.* Toxicological Sciences, 2021. **184**(1): p. 127-141.

APPENDIX A: IMMUNOBLOT IMAGES

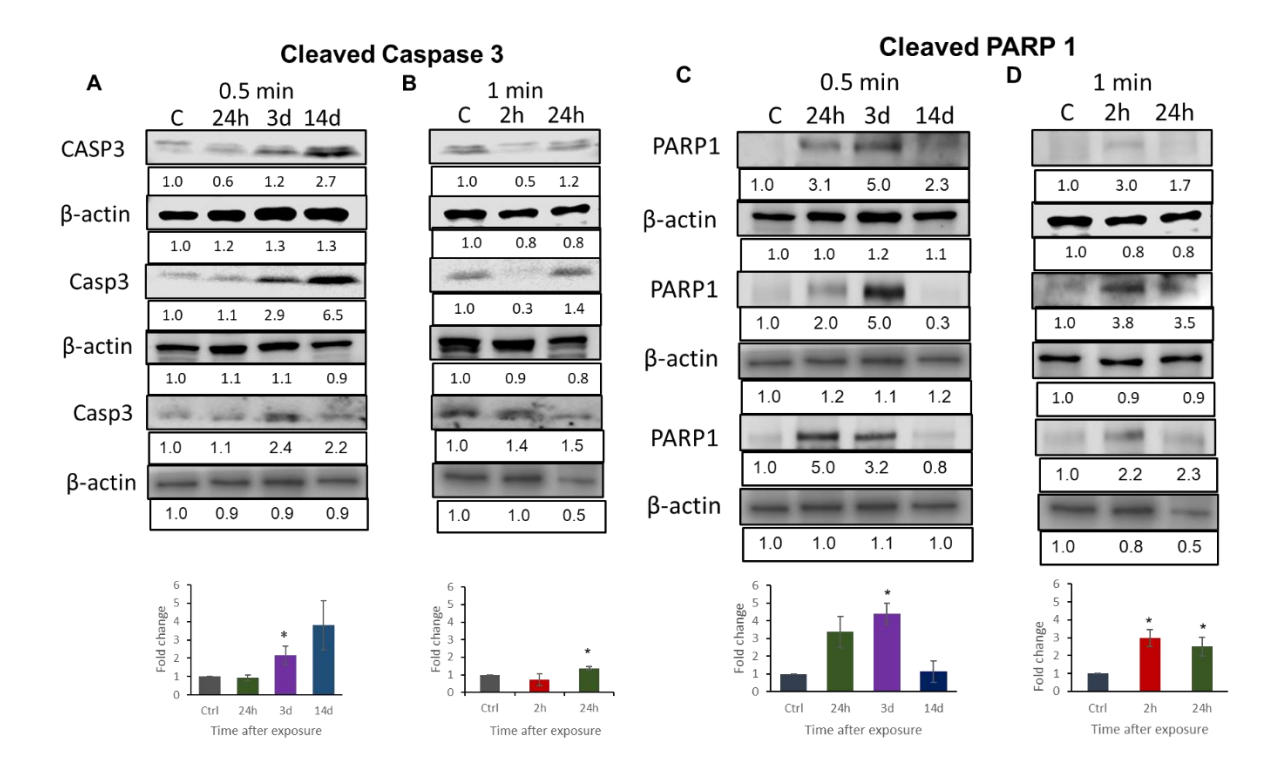


Figure 16: Effect of CX exposure on molecular markers of apoptosis. Presenting immunoblot pictures of all samples showing the level of (A) Cleaved Caspase 3 following 0.5, and (B) following 1 min, (C) Cleaved PARP 1 following 0.5, and (D) following 1 min CX exposure and their quantification compared to the control group; Data presented are mean ±SEM (n=3). *, p <0.05 compared to control.

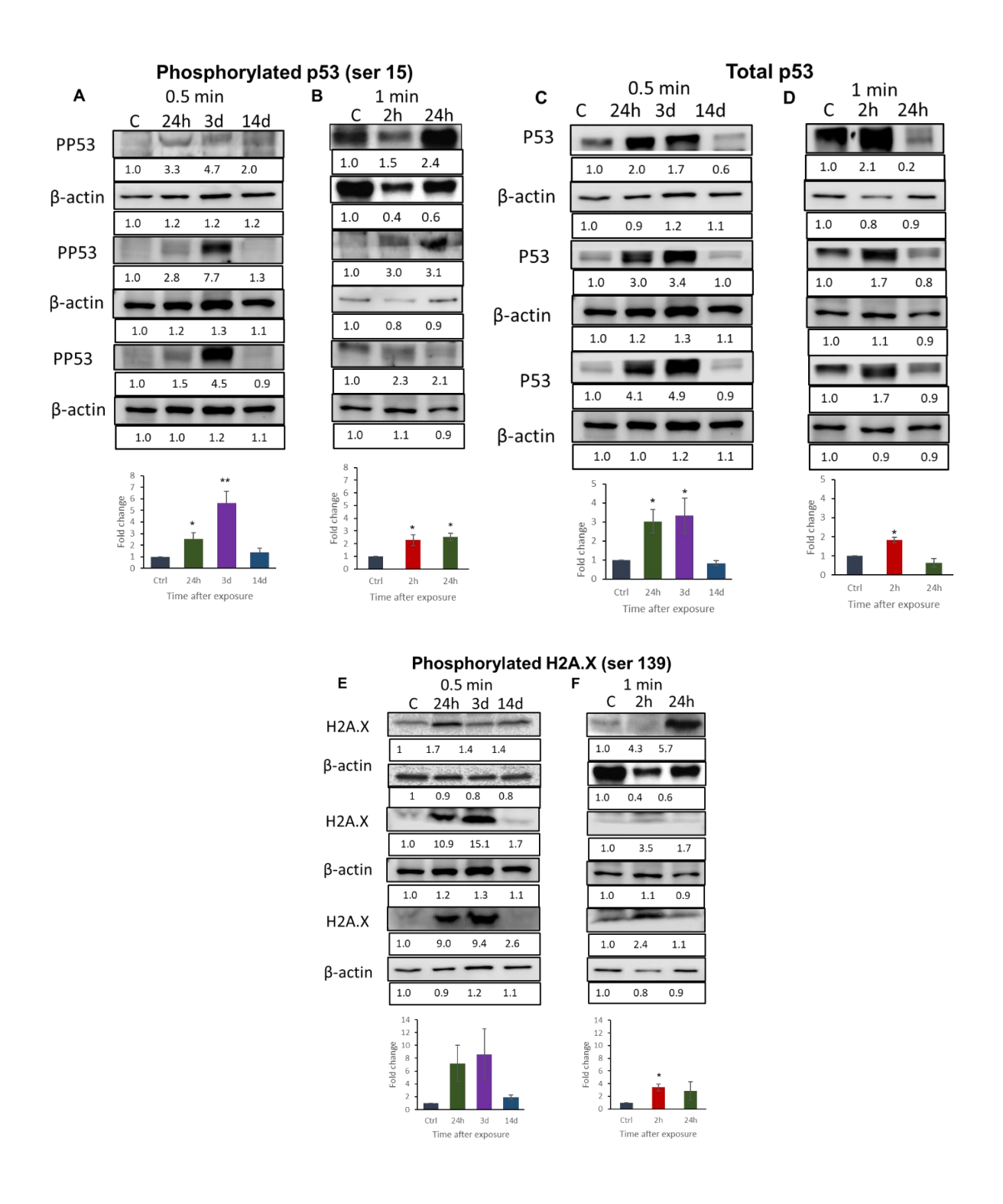


Figure 17: Effect of CX exposure on molecular markers of DNA damage. Presenting immunoblot pictures of all samples showing the level of (A) Phosphorylated p53 (ser15) following 0.5, and (B) following 1 min, (C) total p53 following 0.5, and (D) following 1 min, (E) Phosphorylated H2A.X (ser 139) following 0.5, and (F) following 1 min CX exposure and their quantification compared to the control group; Data presented are mean \pm SEM (n=3). *, p <0.05, **, p <0.01 compared to control.

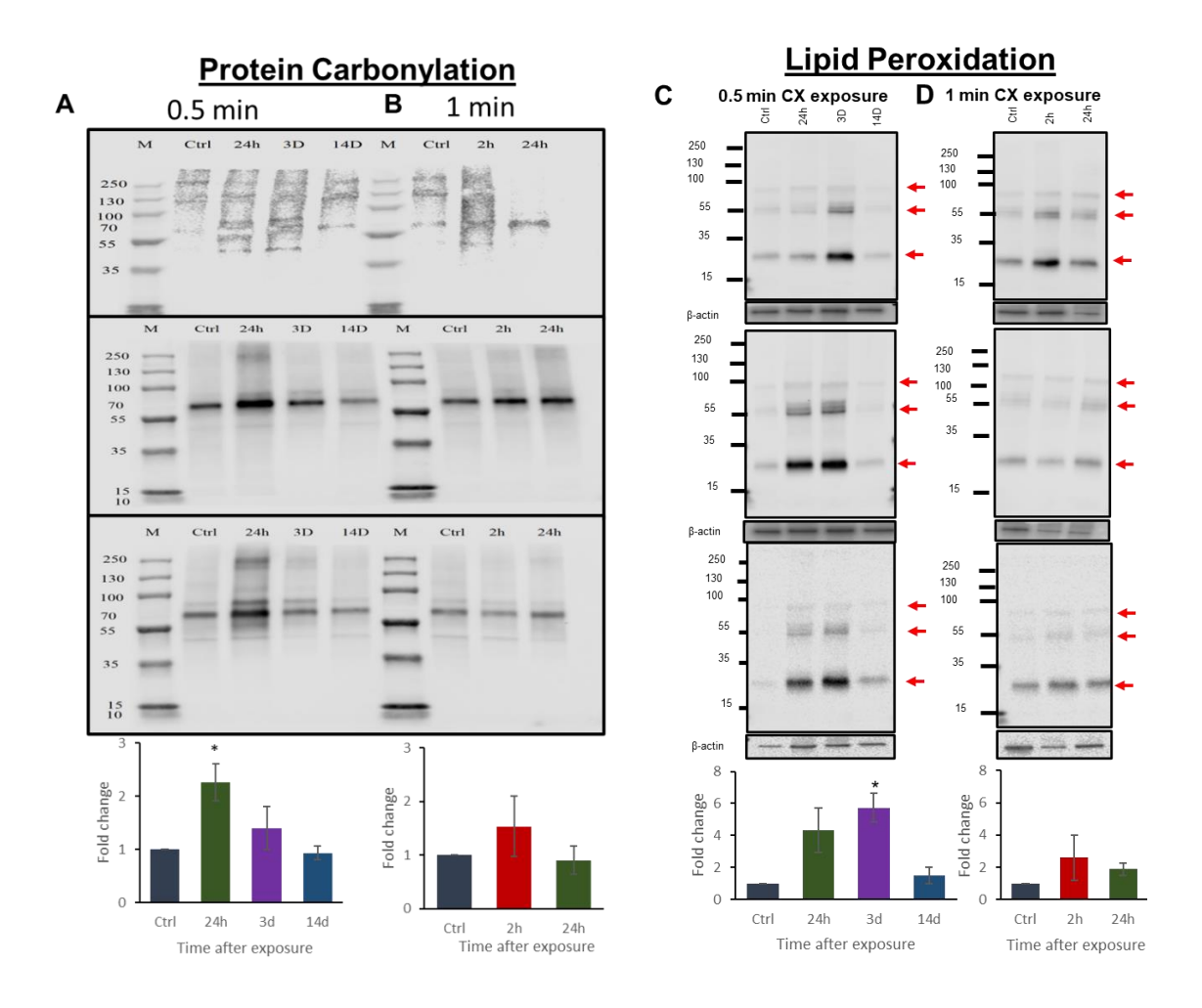


Figure 18: Effect of CX exposure on molecular markers of oxidative stress. Presenting immunoblot pictures of all samples showing the level of (A) protein carbonylation following 0.5, and (B) following 1 min, (C) lipid peroxidation following 0.5, and (D) following 1 min CX exposure and their quantification compared to the control group; Data presented are mean \pm SEM (n=3). *, p <0.05 compared to control.

APPENDIX B: ANALYSIS OF IMMUNOBLOTTING

Sample 3 1 5 3.2 0.8 Sample 3 1 Average 1 3.366667 4.4 1.133333 Average 1 SEM 0 0.876229 0.6 0.600925 SEM 0 0.463 CASP3, 0.5 min CASP3, 1min Phospho p53, 0.5 min Phospho p53, 1 min CAT 24h 3d 14d CAT 25 ample 2 1 2 ample 3 1 2 ample 3 1 2 ample 3 1 2 ample	24h 0.5 1 0.3 1 1.4 1 33 1.3666i 96 0.0881 24h 1.5 2 3 3 3 2.3 2 2.5333	
Sample 1 1 3.1 5 2.3 Sample 1 1 Sample 2 1 2 5 0.3 Sample 2 1 Sample 3 1 5 3.2 0.8 Sample 3 1 Average 1 3.366667 4.4 1.133333 Average 1 SEM 0 0.876229 0.6 0.600925 SEM 0 0.466 SEM 0 0.876229 0.6 0.600925 SEM 0 0.466 CASP3, 0.5 min CASP3, 1min Phospho p53, 0.5 min Phospho p53, 1 min CAT 24 3.2 CAT 24 <td co<="" th=""><th>3 1 1 3 2 2 2 2 3 3 2 2 3 2 3 2 3 1 3 3 1 3 1</th></td>	<th>3 1 1 3 2 2 2 2 3 3 2 2 3 2 3 2 3 1 3 3 1 3 1</th>	3 1 1 3 2 2 2 2 3 3 2 2 3 2 3 2 3 1 3 3 1 3 1
Sample 2 1 2 5 0.3 Sample 2 1 Sample 3 1 5 3.2 0.8 Sample 3 1 Average 1 3.366667 4.4 1.133333 Average 1 SEM 0 0.876229 0.6 0.600925 SEM 0 0.465 CASP3, 0.5 min CASP3, 1min CASP3, 1min CASP3, 1min CASP3, 1min Phospho p53, 0.5 min Phospho p53, 0.5 min Phospho p53, 1 min CASP3, 1min Phospho p53, 0.5 min Phospho p53, 1 min Phospho p53, 0.5 min Phospho p53, 1 min CATI 24h 3 1 1 1 2 2 3 3 1 3 </th <th>24h 24h 1.5 24h 24h 2.5 24h 24h 2.5 24h 2.6 24h 2.5 267 2.5333</th>	24h 24h 1.5 24h 24h 2.5 24h 24h 2.5 24h 2.6 24h 2.5 267 2.5333	
Sample 3 1 5 3.2 0.8 Sample 3 1 Average 1 3.366667 4.4 1.133333 Average 1 SEM 0 0.876229 0.6 0.600925 SEM 0 0.463 CASP3, 0.5 min CASP3, 1min CASP3, 1min CASP3, 1min CASP3, 1min CASP3, 1min CASP3, 1min CASP3, 1min CASP3, 1min CASP3, 1min CASP3, 1min CASP3, 1min CASP3, 1min CASP3, 1min CASP3, 1min Phospho p53, 0.5 min Phospho p53, 1 min Phospho p53, 0.5 min Phospho p53, 1 min CATI 24h 3d 14d CCTI 2h Sample 3 1 1 1 2.53333 5.633333 1.4 Average 1 2.2666	2.2 2 2 3 2 3 2 3 4 4 4 1 1 3 3 1 3 6 6 6 6 9 6 0 .0881 4 2 4 h 2 3 3 3 3 2 3 2 5 6 7 2 .5333 4 2 5 6 7 2 .5333 4 2 5 6 7 2 .5333 4 3 3 3 3 3 3 3 3 3 3 3 3 3 3 3 3 3	
Average 1 3.366667 4.4 1.133333 Average 1 SEM 0 0.876229 0.6 0.600925 SEM 0 0.466 CASP3, 0.5 min CASP3, 1 min Average 1 0.6 1.2 2.7 Sample 2 1 Sample 3 1 1.1 2.4 2.2 Sample 3 1 Average 1 0.933333 2.166667 3.8 Average 1 0.7333 SEM Phospho p53, 0.5 min Phospho p53, 1 min CASP3, 1 min Phospho p53, 1 min CASP3, 1 min Phospho p53, 1 min Phospho p53, 1 min CASP3, 1 min CASP3, 1 min CASP3, 1 min Phospho p53, 1 min CASP3, 1 min C	3 2 24h	
SEM 0 0.876229 0.6 0.600925 SEM 0 0.463 CASP3, 0.5 min CASP3, 1 min Ctrl 24h 3d 14d Ctrl 2h Sample 1 1 0.6 1.2 2.7 Sample 1 1 Sample 2 1 1.1 2.4 2.2 Sample 2 1 Sample 3 1 1.1 2.4 2.2 Sample 3 1 Average 1 0.933333 2.166667 3.8 Average 1 0.733 SEM 0 0.166667 0.504425 1.357694 SEM 0 0.3383 Phospho p53, 0.5 min Phospho p53, 1 min Phospho p53, 1 min Phospho p53, 1 min Ctrl 24h 3d 14d Average 1 2.533333 1.4 Average 1 2.533333 1.4 Average 1 2.2666 SEM 0 0.536449 1.034945 0.321455 SEM 0	24h 0.55 1.0.3 1.4 1.33 1.3666i 96 0.08819 24h 1.5 2 3 3 3 2.3 2 2 67 2.53333	
CASP3, 0.5 min Ctrl 24h 3d 14d Ctrl 2h Sample 1 1 0.6 1.2 2.7 Sample 1 1 1.1 2.9 6.5 Sample 2 1 1.1 2.4 2.2 Sample 3 1 1.1 Average 1 0.33333 2.166667 3.8 Average 1 0.33333 SEM Phospho p53, 0.5 min Phospho p53, 1 min Ctrl 24h 3d 14d Ctrl 2h Sample 2 1 0.73333 Emble 3 Phospho p53, 0.5 min Phospho p53, 1 min Ctrl 24h 3d 14d Ctrl 2h Sample 1 1 1.5 4.5 0.9 Sample 2 1 Sample 2 1 Sample 2 1 Sample 3 1 Average 1 2.533333 1.4 Average 1 2.533333 1.4 Average 1 2.2666 SEM 0 0 0.4333 DF3, 1 min	24h 0.5 1 0.3 1 1.4 1 33 1.3666i 96 0.0881 24h 1.5 2 3 3 3 2.3 2 2.5333	
Ctrl 24h 3d 14d Ctrl 2h	0.5 1 0.3 1 1.4 1 33 1.36666 96 0.08819 24h 1.5 2 3 3 2.3 2 67 2.53333	
Sample 1 1 0.6 1.2 2.7 Sample 1 1 Sample 2 1 1.1 2.9 6.5 Sample 2 1 Sample 3 1 1.1 2.4 2.2 Sample 3 1 Average 1 0.933333 2.166667 3.8 Average 1 0.733 SEM 0 0.166667 0.504425 1.357694 SEM 0 0.338 Phospho p53, 0.5 min Phospho p53, 1 min Phospho p53, 0.5 min Phospho p53, 1 min Phospho p53, 1 min Sample 1 1 1.5 4.5 0.9 Sample 1 1 Sample 3 1 2.8 7.7 1.3 Sample 3 1 Average 1 2.533333 5.633333 1.4 Average 1 2.2666 SEM 0 0.536449 1.034945 0.321455 SEM 0 0.4333 <td colspa<="" td=""><td>0.5 1 0.3 1 1.4 1 33 1.36666 96 0.08819 24h 1.5 2 3 3 2.3 2 67 2.53333</td></td>	<td>0.5 1 0.3 1 1.4 1 33 1.36666 96 0.08819 24h 1.5 2 3 3 2.3 2 67 2.53333</td>	0.5 1 0.3 1 1.4 1 33 1.36666 96 0.08819 24h 1.5 2 3 3 2.3 2 67 2.53333
Sample 1 1 0.6 1.2 2.7 Sample 1 1 Sample 2 1 1.1 2.9 6.5 Sample 2 1 Sample 3 1 1.1 2.4 2.2 Sample 3 1 Average 1 0.933333 2.166667 3.8 Average 1 0.733 SEM 0 0.166667 0.504425 1.357694 SEM 0 0.338 Phospho p53, 0.5 min Phospho p53, 1 min Phospho p53, 0.5 min Phospho p53, 1 min Phospho p53, 1 min Sample 1 1 1.5 4.5 0.9 Sample 1 1 Sample 3 1 2.8 7.7 1.3 Sample 3 1 Average 1 2.533333 5.633333 1.4 Average 1 2.2666 SEM 0 0.536449 1.034945 0.321455 SEM 0 0.4333 <td colspa<="" td=""><td>0.5 1 0.3 1 1.4 1 33 1.36666 96 0.08819 24h 1.5 2 3 3 2.3 2 67 2.53333</td></td>	<td>0.5 1 0.3 1 1.4 1 33 1.36666 96 0.08819 24h 1.5 2 3 3 2.3 2 67 2.53333</td>	0.5 1 0.3 1 1.4 1 33 1.36666 96 0.08819 24h 1.5 2 3 3 2.3 2 67 2.53333
Sample 2 1 1.1 2.9 6.5 Sample 2 1 Sample 3 1 1.1 2.4 2.2 Sample 3 1 Average 1 0.933333 2.166667 3.8 Average 1 0.733333 SEM 0 0.166667 0.504425 1.357694 SEM 0 0.33833333 Phospho p53, 0.5 min Phospho p53, 1 min Phospho p53, 1 min Phospho p53, 1 min 2 1 2 1 2 1 2 1 2 1 2 1 2 1 2 1 2 1 2 3 3 4.7 2 2 3 3 1 4 3 4.7 2 3 3 1 4 <	24h 1.5 2.3 2.3 2.5 2.5 2.5 2.5 2.5 2.5 2.5 2.5 2.5 2.5	
Sample 3 1 1.1 2.4 2.2 Sample 3 1 0.933333 2.166667 3.8 Average 1 0.73333 0.504425 1.357694 SEM 0 0.33833 0.33833 0.504425 1.357694 SEM 0 0.33833 0.33333 0.56647 1.357694 SEM 0 0.33833 0.33333 0.56649 1.357694 SEM 0 0.33833 0.47 0.9 Sample 1 1 1 0.56649 1.034945 0.9 Sample 2 1 1 1 1 0.56649 1.034945 0.321455 SEM 0 0.43333 0.47 0.2 Sample 3 1 0 0.43333 0.321455 SEM 0 0.43333 0.321455 SEM 0 0.43333 0.321455 SEM 0 0.43333 0.34441 0.9 0.9 Sample 3 1 0.2 0.43333 0.4444 0.9 0.9 Sample 3 1 0.0 0.433333 0.833333 0.833333	24h 1.5 2.3 2.3 2.5 2.5 2.5 2.5 2.5 2.5 2.5 2.5 2.5 2.5	
Average 1 0.933333 2.166667 3.8 Average 1 0.7333 SEM 0 0.166667 0.504425 1.357694 SEM 0 0.3383 Phospho p53, 0.5 min Phospho p53, 1 min Ctrl 24h 3d 14d Ctrl 2h Sample 1 1 1.5 4.5 0.9 Sample 1 1 Sample 2 1 2.8 7.7 1.3 Sample 2 1 Sample 3 1 3.3 4.7 2 Sample 3 1 Average 1 2.533333 5.633333 1.4 Average 1 2.2666 SEM 0 0.536449 1.034945 0.321455 SEM 0 0.4333 P53, 0.5 min P53, 0.5 min p53, 1 min Ctrl 24h 3d 14d Ctrl 2h Sample 1 1 4.1 4.9 0.9 Sample 1 1 Sample 2 1 3 3.4 1 Sample 2 1 Sample 3 1 2 1.7 0.6 Sample 1 1 Sample 3 1 2 1.7 0.6 Sample 2 1 Sample 3 1 2 1.7 0.6 Sample 1 1 Sample 3 1 0.0 Average 1 1.8333 SEM 0 0.606447 0.924362 0.120185 SEM 0 0.13333 PH2A.X, 0.5 min PH2A.X, 1 min Ctrl 24h 3d 14d Sample 1 1.8333 SEM 0 0.606447 0.924362 0.120185 SEM 0 0.13333 Average 1 1.8333 SEM 0 0.606447 0.924362 0.120185 SEM 0 0.13333 Average 1 1.8333 SEM 0 0.606447 0.924362 0.120185 SEM 0 0.13333	33 1.3666i 96 0.0881! 24h 1.5 2 3 3 2.3 2 67 2.5333:	
SEM 0 0.166667 0.504425 1.357694 SEM 0 0.3383 Phospho p53, 0.5 min Phospho p53, 1 min Ctrl 24h 3d 14d Ctrl 2h Sample 1 1 1.5 4.5 0.9 Sample 1 1 Sample 2 1 2.8 7.7 1.3 Sample 2 1 Sample 3 1 3.3 4.7 2 Sample 3 1 Average 1 2.533333 5.633333 1.4 Average 1 2.2666 SEM 0 0.536449 1.034945 0.321455 SEM 0 0.4333 p53, 0.5 min p53, 1 min Ctrl 24h 3d 14d Ctrl 2h Sample 1 1 1 4.1 4.9 0.9 Sample 1 1 Sample 2 1 3.33333 3.833333 Average 1 1.83	24h 1.5 2 3 3 2.3 2 67 2.5333	
Ctrl 24h 3d 14d Ctrl 2h Sample 1 1 1.5 4.5 0.9 Sample 1 1 Sample 2 1 2.8 7.7 1.3 Sample 2 1 Sample 3 1 2.533333 5.633333 1.4 Average 1 2.2666 SEM 0 0.536449 1.034945 0.321455 SEM 0 0.4333 p53, 0.5 min p53, 1 min	1.5 2 3 3 2.3 2 67 2.5333	
Ctrl 24h 3d 14d Ctrl 2h Sample 1 1 1.5 4.5 0.9 Sample 1 1 Sample 2 1 2.8 7.7 1.3 Sample 2 1 Sample 3 1 2.533333 5.633333 1.4 Average 1 2.2666 SEM 0 0.536449 1.034945 0.321455 SEM 0 0.4333 p53, 0.5 min p53, 1 min	1.5 2 3 3 2.3 2 67 2.5333	
Sample 1 1 1.5 4.5 0.9 Sample 1 1 Sample 2 1 2.8 7.7 1.3 Sample 2 1 Sample 3 1 3.3 4.7 2 Sample 3 1 Average 1 2.533333 5.633333 1.4 Average 1 2.2666 SEM 0 0.536449 1.034945 0.321455 SEM 0 0.4333 p53, 0.5 min p53, 1 min Ctrl 24h 3d 14d Ctrl 2h Sample 1 1 4.1 4.9 0.9 Sample 1 1 Sample 2 1 3 3.4 1 Sample 2 1 Sample 3 1 2 1.7 0.6 Sample 3 1.0 Average 1 3.033333 3.333333 0.833333 Average 1 1.8333 SEM 0 0.606447 0.924362 0.120185 SEM 0 0.1333 pH2A.X,	1.5 2 3 3 2.3 2 67 2.5333	
Sample 2 1 2.8 7.7 1.3 Sample 2 1 Sample 3 1 3.3 4.7 2 Sample 3 1 Average 1 2.533333 5.633333 1.4 Average 1 2.2666 SEM 0 0.536449 1.034945 0.321455 SEM 0 0.4333 p53, 0.5 min p53, 1 min Ctrl 24h 3d 14d Ctrl 2h Sample 1 1 4.1 4.9 0.9 Sample 1 1 Sample 2 1 3 3.4 1 Sample 2 1 Sample 3 1 2 1.7 0.6 Sample 3 1.0 Awerage 1 3.033333 3.333333 0.8333333 Average 1 1.8333333 SEM 0 0.606447 0.924362 0.120185 SEM 0 0.133333 SEM 0 0.606447 0.924362 0.120185 SEM 0 0.1333333 PH2A.X, 0.5 min <td c<="" td=""><td>3 3 2.3 2 67 2.5333</td></td>	<td>3 3 2.3 2 67 2.5333</td>	3 3 2.3 2 67 2.5333
Sample 3 1 3.3 4.7 2 Sample 3 1 2.533333 1.4 Average 1 2.2666 2.266	2.3 2 67 2.5333	
Average 1 2.533333 5.633333 1.4 Average 1 2.266t SEM 0 0.536449 1.034945 0.321455 SEM 0 0.4333 p53, 0.5 min p53, 1 min p53, 1 min	67 2.5333	
SEM 0 0.536449 1.034945 0.321455 SEM 0 0.4333 p53, 0.5 min p53, 1 min Ctrl 24h 3d 14d Ctrl 2h Sample 1 1 4.1 4.9 0.9 Sample 1 1 Sample 2 1 3 3.4 1 Sample 2 1 Sample 3 1 2 1.7 0.6 Sample 3 1.0 Awerage 1 3.033333 3.333333 Average 1 1.833 SEM 0 0.606447 0.924362 0.120185 SEM 0 0.1333 pH2A.X, 0.5 min pH2A.X, 1 min Ctrl 24h 3d 14d Ctrl 2h Sample 1 1 1.7 1.4 1.4 Sample 1 1 Sample 2 1 9 9.4 2.6 Sample 3 1 Sample 3		
p53, 0.5 min p53, 1 mi	33 0 2962	
Ctrl 24h 3d 14d Ctrl 2h Sample 1 1 4.1 4.9 0.9 Sample 1 1 Sample 2 1 3 3.4 1 Sample 2 1 Sample 3 1 2 1.7 0.6 Sample 3 1.0 Awerage 1 3.033333 3.333333 Average 1 1.8333 SEM 0 0.606447 0.924362 0.120185 SEM 0 0.1333 pH2A.X, 0.5 min pH2A.X, 1 min Ctrl 24h 3d 14d Ctrl 2h Sample 1 1 1.7 1.4 1.4 Sample 1 1 Sample 2 1 9 9.4 2.6 Sample 2 1 Sample 3 1 10.9 15.1 1.7 Sample 3 1	33 0.2302	
Sample 1 1 4.1 4.9 0.9 Sample 1 1 Sample 2 1 3 3.4 1 Sample 2 1 Sample 3 1 2 1.7 0.6 Sample 3 1.0 Awerage 1 3.033333 3.333333 Average 1 1.833333333 SEM 0 0.606447 0.924362 0.120185 SEM 0 0.1333333 pH2A.X, 0.5 min pH2A.X, 1 min Ctrl 24h 3d 14d Ctrl 2h Sample 1 1 1.7 1.4 1.4 Sample 1 1 Sample 2 1 9 9.4 2.6 Sample 2 1 Sample 3 1 10.9 15.1 1.7 Sample 3 1		
Sample 1 1 4.1 4.9 0.9 Sample 1 1 Sample 2 1 3 3.4 1 Sample 2 1 Sample 3 1 2 1.7 0.6 Sample 3 1.0 Awerage 1 3.033333 3.333333 Average 1 1.833333333 SEM 0 0.606447 0.924362 0.120185 SEM 0 0.1333333 pH2A.X, 0.5 min pH2A.X, 1 min Ctrl 24h 3d 14d Ctrl 2h Sample 1 1 1.7 1.4 1.4 Sample 1 1 Sample 2 1 9 9.4 2.6 Sample 2 1 Sample 3 1 10.9 15.1 1.7 Sample 3 1	24h	
Sample 2 1 3 3.4 1 Sample 2 1 Sample 3 1 2 1.7 0.6 Sample 3 1.0 Awerage 1 3.033333 3.333333 Average 1 1.8333333 SEM 0 0.606447 0.924362 0.120185 SEM 0 0.133333 pH2A.X, 0.5 min pH2A.X, 1 min Ctrl 24h 3d 14d Ctrl 2h Sample 1 1 1.7 1.4 1.4 Sample 1 1 Sample 2 1 9 9.4 2.6 Sample 2 1 Sample 3 1 10.9 15.1 1.7 Sample 3 1	2.1 0	
Sample 3 1 2 1.7 0.6 Sample 3 1.0 Awerage 1 3.033333 3.333333 Average 1 1.833333333 SEM 0 0.606447 0.924362 0.120185 SEM 0 0 0.133333 pH2A.X, 0.5 min pH2A.X, 1 min Ctrl 24h 3d 14d Ctrl 2h Sample 1 1 1.7 1.4 1.4 Sample 1 1 Sample 2 1 9 9.4 2.6 Sample 2 1 Sample 3 1 10.9 15.1 1.7 Sample 3 1	1.7 0	
Awerage 1 3.033333 3.333333 0.833333 Average 1 1.8333 SEM 0 0.606447 0.924362 0.120185 SEM 0 0 0.1333 pH2A.X, 0.5 min pH2A.X, 1 min pH2A.X,	1.7 0	
SEM 0 0.606447 0.924362 0.120185 SEM 0 0.1333 pH2A.X, 0.5 min pH2A.X, 1 min Ctrl 24h 3d 14d Ctrl 2h Sample 1 1 1.7 1.4 1.4 Sample 1 1 Sample 2 1 9 9.4 2.6 Sample 2 1 Sample 3 1 10.9 15.1 1.7 Sample 3 1		
Ctrl 24h 3d 14d Ctrl 2h Sample 1 1 1.7 1.4 1.4 Sample 1 1 Sample 2 1 9 9.4 2.6 Sample 2 1 Sample 3 1 10.9 15.1 1.7 Sample 3 1		
Ctrl 24h 3d 14d Ctrl 2h Sample 1 1 1.7 1.4 1.4 Sample 1 1 Sample 2 1 9 9.4 2.6 Sample 2 1 Sample 3 1 10.9 15.1 1.7 Sample 3 1		
Sample 1 1 1.7 1.4 1.4 Sample 1 1 Sample 2 1 9 9.4 2.6 Sample 2 1 Sample 3 1 10.9 15.1 1.7 Sample 3 1		
Sample 2 1 9 9.4 2.6 Sample 2 1 Sample 3 1 10.9 15.1 1.7 Sample 3 1	24h	
Sample 3 1 10.9 15.1 1.7 Sample 3 1	2.4 1	
P P P P P P P P P P P P P P P P P P P	3.5 1	
	1.3 5	
Average 1 7.2 8.633333 1.9 Average 1	3.4 2.8333	
SEM 0 2.804164 3.973384 0.360555 SD 0 0.550	57 1.4437	
PC, 0.5 min PC, 1 min		
Ctrl 24h 3d 14d Ctrl 2h	24h	
Sample 1 1.0 1.7 2.2 1.2 Sample 1 1	2.6	
	1.3 1	
•).7 0	
Average 1.0 2.3 1.4 0.9 Average 1 1.5333		
	53 0.2645	
LP, 0.5 min LP, 1 min		
Ctrl 24h 3d 14d Ctrl 2h	24h	
	5.4 2	
	1	
·	L.4 1	
	2.6 1	
SEM 0 1.386042 0.920748 0.503322 SEM 0 1.404	54 0 3785	

Figure 19: Excel sheet and analysis of average fold change and Standard Error of Mean (SEM) for immunoblot of molecular markers of all samples in this study.